

ABSTRACT

Title of Thesis: CELLULOSE NANOPAPER: A STUDY OF COMPOSITION AND SURFACE MODIFICATIONS TO DEVELOP SUSTAINABLY-SOURCED ALTERNATIVES TO PLASTICS

Authors: Karena Bucu, Eddie Chang, Parisa Davoodi, Julia Downing, Delena Ganey, Brandon Green, Jonathan Kagan, Sachi Khemka, Erik Larmore, Hannah Russell, Thomas Schmitt, Luke Travisano, Jeannette Van Sickle, Jenshinn Stacy Wang

Directed by: Dr. Liangbing Hu, Associate Professor, Department of Materials Science and Engineering, University of Maryland Energy Research Center (UMERC)

Pollution from the fossil-fuel-powered production of plastics presents a serious threat to the planet's environmental health. To address this issue, cellulose nanopaper (CNP) has been pushed as an abundant, sustainably-sourced potential alternative. Initially derived from wood pulp, CNP is comprised of a network of nanosized cellulose fibers. Although CNP has exhibited remarkable optical transparency, porosity, and stiffness, the need for improvement in its chemical and electrical properties has been identified. Optimizing these properties would allow CNP to function in flexible electronic systems. By altering the paper through several surface processing experiments, the most effective treatments to increase CNP's functionality were identified. These treatments included altering the source of cellulose, performing atomic layer deposition (ALD) with Al_2O_3 , conducting surface esterification reactions, and applying transparent, conductive coatings. Along with conventional pine fibers, CNP with longer cellulose fibers from the jute plant was developed. Sequential, uniform deposition of Al_2O_3 films via ALD was

also implemented for added stability. The surface of the CNP was treated with organic acids to yield nonpolar ester groups, with the goal of increasing water resistance. Finally, conductive ink coatings consisting of carbon nanotubes and cellulose nanofibers demonstrated improved electrical conductivity of CNP for optoelectronic applications. After the treatments, material properties were characterized, including strength, flexibility, water resistance, conductivity, surface smoothness, and transparency. Improvements in hydrophobicity, conductivity, and surface smoothness were observed. These treatments and their corresponding findings represent promising ways of improving the functionality of CNP without dramatically altering its high transparency and flexibility.

**CELLULOSE NANOPAPER: A STUDY OF COMPOSITION AND SURFACE
MODIFICATIONS TO DEVELOP SUSTAINABLY-SOURCED
ALTERNATIVES TO PLASTICS**

by

Team NATURE: Nanopaper Applications to Universalize Renewable Electronics

Karenn Buco, Eddie Chang, Parisa Davoodi, Julia Downing, Delena Ganey,
Brandon Green, Jonathan Kagan, Sachi Khemka, Erik Larmore, Hannah Russell,
Thomas Schmitt, Luke Travisano, Jeannette Van Sickle, Jenshinn Stacy Wang

Mentor: Dr. Liangbing Hu, Associate Professor, Department of Materials Science and
Engineering, University of Maryland Energy Research Center (UMERC)

Librarian: Ms. Nevenka Zdravkovska

Thesis submitted in partial fulfillment of the requirements of the Gemstone Program
University of Maryland 2017

Advisory Committee:
Dr. Liangbing Hu, Mentor
Dr. Tian Li
Dr. Jeffrey Gilman
Dr. Ian White
Mr. Alex Pearse

© Copyright by

Team NATURE

Karenn Buco, Eddie Chang, Parisa Davoodi, Julia Downing, Delena Ganey,
Brandon Green, Jonathan Kagan, Sachi Khemka, Erik Larmore, Hannah Russell,
Thomas Schmitt, Luke Travisano, Jeannette Van Sickle, Jenshinn Stacy Wang

2017

Acknowledgements

We thank our mentor, Dr. Liangbing Hu, for all his educational support, countless hours of time, and dedication to our research project. We also thank the BingNano group at UMERG and our wonderful teaching assistants, Yonggang Yao and Nathaniel Jang, for their assistance and guidance. Thank you also to Dr. Frank Coale, Dr. Kristen Skendall, and the rest of the Gemstone staff for their constant support. We thank our thesis proposal and defense panel members: Dr. Raymond Phaneuf, Dr. Jeremy Munday, Dr. Tian Li, Dr. Jeffrey Gilman, Dr. Ian White, and Alex Pearse. We thank our librarians, Robin Dasler and Nevenka Zdravkovska, for their meetings and research advice. We thank the donors and staff that contributed to the success of our LaunchUMD campaign, and the Sustainability Grant for helping us fund our research. Finally, we thank our friends and families for supporting us throughout the duration of this project.

Table of Contents

Acknowledgements.....	ii
Table of Contents	iii
List of Figures	iv
List of Tables	v
Chapter 1. Introduction	1
Chapter 2. Mechanical and Optical Characterization of Jute-Based Cellulose Nanopaper	5
Abstract	5
Introduction.....	5
Methodology	8
Results and Discussion	9
Conclusion	14
Future Research	14
Chapter 3. Atomic Layer Deposition of Al ₂ O ₃ to Improve Various Properties of Transparent Nanopaper	15
Abstract	15
Introduction.....	16
Methodology	20
Results and Discussion	22
Conclusion	25
Future Research	25
Chapter 4. Water Stability Improvements to Cellulose Nanopaper through Surface Reactions.....	26
Abstract	26
Introduction.....	27
Methodology	31
Results and Discussion	34
Conclusion	40
Future Research	41
Chapter 5. Scalable Carbon Nanotube/Cellulose Nanofiber Coatings on Cellulose Nanopaper and Derivatives	43
Abstract	43
Introduction.....	44
Methodology	48
Results and Discussion	54
Conclusion	63
Future Research	63
Chapter 6. Conclusion.....	65
References.....	71
Appendices.....	79
Appendix A: Cellulose Nanopaper (CNP) Fabrication	79
Appendix B: Atomic Layer Deposition (ALD) Process Specifications	80
Appendix C: Carbon Nanotube (CNT) Ink Formula and Preparation	81
Glossary	82

List of Figures

Figure 1.1: Image of cellulose nanopaper (CNP).	2
Figure 2.1: Visual comparison of jute and pine CNP.	10
Figure 2.2: Optical microscope images of jute CNP topology.	10
Figure 2.3: Atomic Force Microscopy (AFM) image of pine cellulose fibers.	12
Figure 2.4: Three-dimensional AFM imagery of pine CNP.	12
Figure 3.1: SEM image of CNP cross section.	17
Figure 3.2: Schematic of the four stages of ALD.	19
Figure 3.3: SEM cross section of CNP treated with 250 cycles of ALD.	22
Figure 3.4: SEM cross section of CNP treated with 500 cycles of ALD.	23
Figure 3.5: Stress-strain curves comparison for ALD and standard CNP samples.	24
Figure 4.1: Generic carboxylic acid esterification reaction.	28
Figure 4.2: Reaction of alcohol groups on CNP.	28
Figure 4.3: Contact angle measurements for ALD-treated nanopaper.	33
Figure 4.4: Contact angle over 15 minutes one day after reaction.	36
Figure 4.5: Contact angle over 15 minutes 120 days after reaction.	37
Figure 4.6: Contact angle over 15 minutes 1 day after reaction.	37
Figure 4.7: Contact angle over 15 minutes 120 days after reaction.	38
Figure 4.8: Combined FTIR Spectra of treated CNP.	40
Figure 5.1: Fabrication and coating of CNT ink.	51
Figure 5.2: SEM cross-sections of ink coatings and topology.	52
Figure 5.3: Hall Effect measurement system and sheet resistance results.	53
Figure 5.4: SEM cross-sections of the CNP substrate.	55
Figure 5.5: Transmittance measurements for all sample types.	57
Figure 5.6: Sheet resistance versus transmittance for all samples.	58

List of Tables

Table 1.1: Comparison of CNP to traditional paper and plastic.	3
Table 3.1: Young's modulus of ALD and control CNP samples.	24
Table 4.1: Organic acids used in esterification reaction.	30
Table 4.2: Water absorption as a percentage of mass of sample.	35
Table 5.1: Summary of CNP specimens coated with inks.	48
Table 5.2: Paired T-test: Difference of Means (Sheet Resistance).	59
Table 5.3: Paired T-test: Difference of Means (Transmittance).	60

Chapter 1. Introduction

Today's technologically driven society has fostered a growing global dependence on flexible plastic components in electronics. Industry-standard plastics, such as polyethylene terephthalate (PET), are relatively lightweight, low-cost, and moldable, making them convenient alternatives to metals and ceramics in material production. Manufacturers implement them in solar cells, television displays, smartphone touchscreens, batteries, etc. However, thin plastic films can take thirty years to degrade, and more common plastic components can last up to 450 years (Zhu et al., 2013 [EES]). The disposal of these plastics in landfills consumes limited natural resources such as land and fossil fuels (Hopewell et al., 2009). While convenient for short-term use, plastic waste products act as rampant pollutants that pose daunting environmental concerns. In particular, plastics in the oceans pose a major ecological concern for the species living there. Since plastics cannot be broken down easily by chemical or biological means, they are shredded by waves in the ocean to create microplastics. These microplastics are then bioaccumulated in the ecosystem and ingested by animals.

One potential alternative to plastic films is a highly transparent material composed of a network of cellulose-based polymers, known as cellulose nanopaper (CNP), shown in Figure 1.1. CNP has demonstrated promise as a replacement for plastic in devices like touchscreens and television displays because of its ability to compete with industry standards, like PET, in terms of mechanical, thermal, optical and electrical properties (Zhu et al., 2013 [Nanoscale]).



Figure 1.1: A piece of cellulose nanopaper, alongside traditional paper used for printing.

Table 1.1 indicates that CNP has a tensile strength ranging from 100-200 MPa, which is higher than that of PET. The transmittance of PET and CNP is equivalent, which shows that CNP can compete with similar industrial competitors for electronic displays. Furthermore, CNP is a suitable candidate for sustainable mass production, because cellulose is naturally abundant, biodegradable, versatile, and inexpensive. Phasing out plastics with CNP would reduce plastic-based pollution and preserve nonrenewable resources used in manufacturing and plastic disposal processes.

Table 1.1: Comparison of optical, mechanical and sustainable characteristics of CNP to those of traditional paper and plastic (Zhu et al., 2014).

Characteristics	Nanopaper	Traditional Paper	Plastic
Transmittance at 550 nm (%)	90	20	90
Ultimate Tensile Strength (MPa)	200-400	6	50
Renewability	High	High	Low

A **life cycle assessment** performed on paper and plastic products depends greatly on the waste management strategy implemented at the end of use. However, the production of plastics emits similar or slightly higher amounts of greenhouse gases as the production of paper (Hunt, 1995). CNP also has more options for reuse, post-consumption than most plastics. In 2012, 45.6 million tons of damaged, obsolete, or unwanted electronics were discarded (Lee, 2016). Most plastics within these electronics are derived from petroleum, which degrade on the scale of hundreds of years and cannot be composted. Some plastics can be recycled, but it depends greatly on the type of polymer used. CNP on the other hand, could be composted easily since it is made entirely of cellulose and can also be recycled or burned to release energy. Due to these factors, CNP was determined to be more eco-friendly than plastics.

However, CNP is a relatively novel material, and few avenues to improve crucial mechanical, chemical, and electrical properties have been explored. Key areas of research regarding CNP’s potential electronic applications include improving its mechanical properties, water stability, and optical transparency. While adapting and applying transparent nanopaper to touchscreens, light emitting diodes, solar cells, printable electronics, and batteries would allow the material to become more

appealing as a mainstream alternative to plastics, these applications would also require fortification of the material's nanostructure.

Thus, the central research question of this study is: *Which properties of cellulose nanopaper can be enhanced, and what strategies are most effective for optimizing CNP for use in electronics and other applications?* To answer this research question, four parallel and synergistic research processes were employed to ultimately create a superior version of CNP by improving its mechanical, chemical, and conductive properties. The first process altered CNP's cellulose source from the conventional softwood pine to the jute plant. The second process utilized self-limiting conformal deposition of alumina to strengthen the CNP nanostructure. The third process aimed to induce hydrophobicity through surface esterification reactions. Lastly, the fourth process applied conductive carbon nanotube (CNT) coatings to lower overall sheet resistance for potential use in electronic applications.

The CNP was then evaluated on many criteria to see how these treatments affected the targeted properties. Most post-processing property tests were used to characterize samples from multiple treatments so that the effects from different composition and surface modifications could be recognized. In this way, the four processes were ultimately unified to contribute to a globalized view of how CNP can not only be incorporated into existing technologies, but also further developed for use in novel technologies.

Chapter 2. Mechanical and Optical Characterization of Jute-Based Cellulose Nanopaper

Abstract

Cellulose nanopaper (CNP) is a highly transparent material, with a **bending radius** of 1mm, and a **tensile strength** of up to 200 MPa. With its incredible mechanical, thermal, and optical properties, CNP has the potential to replace plastic films in electronic applications. Currently, CNP is made from softwood pine fibers which, when broken down, range from 5-10 nm in diameter. Jute cellulose has been largely unexplored as a starting material for CNP. Jute **cellulose** fibers possess many advantages that include low density, low cost, high cellulose content, and longer molecular chains. The existing pine CNP manufacturing procedure is used on jute fibers and evaluated through tensile testing and optical transmittance measurements to determine the differences in mechanical strength, optical properties, and flexibility. Jute CNP was found to be brittle, non-homogeneous, opaque, and yellow in color.

Introduction

Typically, cellulose nanopaper is fabricated using softwood fibers, which have greater strength and lower costs than hardwood fibers (Stelte & Stanadi, 2009). Individual softwood microfibrils vary in size from 20 to 40 μm in diameter and 1 to 3 mm in length (Zhu et al., 2013 [Nanoscale]). CNP is composed of cellulose nanofibrils (CNF), typically 5-10 nm in diameter, which are obtained from wood pulp using a disintegration process that involves multiple mechanical and chemical treatments. Fundamentally, CNP has a highly porous, layered microstructure that

makes it unique among transparent substrates. The networked structure is layered and densely packed with **hydrogen bonding** between the fibers, which contribute to the material's high strength as well as a high degree of flexibility. Current generation CNP has a maximum tensile strength value of ~200 MPa, occurring at 19% **porosity** (Zhu et al., 2014). This ratio of tensile strength and flexibility is ideal for **roll-to-roll printing** and 3D structure applications. A study by Zhu, et al. shows that CNP, like regular paper, has a very low bending radius, allowing it to fold and mold easily (Zhu et al., 2013 [Nanoscale]). Compared to CNP's bending radius of 1 mm, plastics of similar thickness have a bending radius of ~5 mm, indicating that CNP is more flexible and foldable compared to plastic (Huang et al., 2013). The fibrous and porous layered structure present within CNP gives it excellent flexibility with a typical pore size between 10-50 nm and allows it to release the stress in the layers affected while bending in an electronic device (Zhu et al., 2013 [Nanoscale]).

While nanopaper with at least 60% transmittance is deemed transparent, CNP with **transmittance** exceeding 90% has been developed (Zhu et al., 2013 [Nanoscale]). Improving transparency can be achieved by removing gaps between fibers and increasing surface smoothness, as well as by using different cellulose sources and methods to process CNFs. Increasing **packing density** and eliminating pores between constituent fibers reduces the amount of light **scattering** that occurs, and thus improves transmittance and allows more light to pass through the material (Fang et al., 2013). When using a TEMPO/NaBr/NaClO **oxidation** system, hydroxyl groups are converted to carboxylic groups. Compared to unmodified fibers, **TEMPO-oxidized** fibers are shorter, experience swelling, and exhibit a lower **degree of**

polymerization. The swelled fibers are then broken down to nanofibers using a high-pressure homogenizer, reducing the fiber diameters. Thus, the amount of light scattering is reduced, more light can pass through, and the CNP exhibits favorable optical properties.

Despite these promising results, CNP's overall mechanical properties must be improved before it can be implemented in more robust applications. Overall transparency must be maintained for CNP to remain suitable in touchscreen, solar cells, and related applications. One strategy for improving CNP's mechanical strength is to explore alternate cellulose source materials, as this provides the potential to lower production costs while creating a more desirable form of CNP. Jute, a biodegradable fiber traditionally used to manufacture carpets, ropes, and canvas, is a possible alternative (Wang et al., 2009). Jute fiber is the second most-produced cellulosic fiber after cotton. It is typically harvested two to three times annually, meaning it is abundant, relatively inexpensive, and easy to obtain (Cao et al., 2014). Jute fiber naturally possesses long strands, a property that has the potential to improve CNP's mechanical properties (Wang et al., 2009). Its low density, high **microfibril angle**, and cellulose content of up to 71.5% make it ideal for CNF extraction, compared to softwood fibers, which typically have cellulose content between 40 and 45% (Yu et al., 2014).

Spherical and elliptical-shaped jute nanofibers (JNF) have been extracted with diameters in the range of 50-120 nm, which notably exceed the diameter of softwood CNF by more than two times (Das et al., 2010). JNFs used to reinforce a **biocopolyester** matrix at 10 wt% were found to increase the composite's tensile

strength by 20% (Das et al., 2010). Jute fibers possess a large quantity of hydroxyl groups, which allow them to interact well with the biocopolyester matrix's polar ester links. Composites have also exhibited improved flexural mechanical properties when reinforced with jute fibers that had been treated with 5% NaOH solution (Sinha & Rout, 2009). Alkali treatments have been found to remove **hemicelluloses** and **lignin** from jute cellulose, allowing the fibers to exhibit closer packing density. With the addition of TEMPO-oxidation and mechanical homogenization, jute cellulose nanowhiskers can be produced with diameters as thin as 3-10 nm (Cao et al., 2014).

There are currently limited studies that have demonstrated the effects of using jute fiber to produce CNP. While the properties of jute nanopaper are expected to be like those of wood fibers, they remain largely unknown. Existing optimized CNP has exhibited maximum tensile strength of ~200 MPa at 19% porosity, and transmittance exceeding 90% (Zhu et al., 2014, Zhu et al., 2013 [Nanoscale]). Therefore, optimized jute CNP should demonstrate comparable values to pine CNP. The production of nanopaper samples derived from jute fibers demonstrated how a change in source material affects the fundamental mechanical and optical characterization of nanopaper.

Methodology

Cellulose Nanofiber Preparation. The process for breaking down cellulose microfibrils into their elementary nanofibers is a combination of chemical and physical treatments. In a buffer solution composed of sodium carbonate and sodium bicarbonate, the wet pulp was mixed with TEMPO ((2,2,6,6-tetramethylpiperidin-1-yl)oxidanyl), an oxidant that greatly increases the negative charge of the cellulose

chain. The resulting swelling allows for enhanced physical decomposition of the fibers. The solution was sent through a microfluidizer, which at a pressure upwards of 40,000 psi shears the fibers into elementary constituents on the order magnitude of 50 nm diameter. The resulting suspension was then re-dispersed in water and was ready to be cast in a humidity control chamber. Refer to Appendix A for the detailed instructions with appropriate chemical ratios and step times.

Results and Discussion

Jute CNP, prepared by applying the pine CNP procedure to jute cellulose fibers, resulted in properties that notably differed from those of pine CNP. As evident in Figure 2.1, jute CNP exhibited opacity and inhomogeneity, whereas pine CNP was uniformly transparent. The white impurities in the jute CNP reflected pieces of fibers that were not effectively broken-down and dispersed throughout the solution prior to casting. The **topology** of jute CNP is displayed in the optical microscope image in Figure 2.2, in which a variation of fiber dimensions is visible. It was expected, upon creation of the jute fiber solution, that the jute CNP would be opaque due to the milky white appearance of the prepared solution in comparison to the nearly transparent pine fiber solution. The jute CNP also exhibited a yellowish hue, which was not evident in the solution but rather became apparent during the casting stage of the procedure. These characteristics hindered the ability to yield conclusive transmittance results, which were measured on a Perkin-Elmer Lambda 25 UV/Vis **spectrophotometer** for wavelengths in the range of 200 nm to 700 nm. The **inhomogeneity** of the jute CNP disrupted the light transmittance, resulting in unsteady measurements that are unable to be used for discussion.

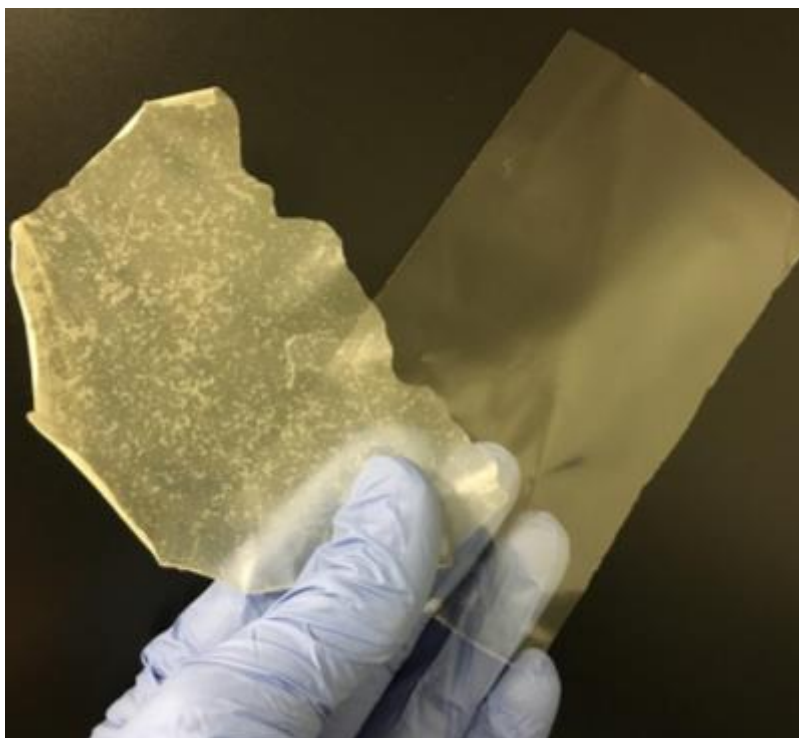


Figure 2.1: Photo of jute CNP (left) and pine CNP (right) side-by-side. Jute CNP is opaque and non-homogenous with chipped edges in comparison to the transparent, homogenous, and clean-cut pine CNP.

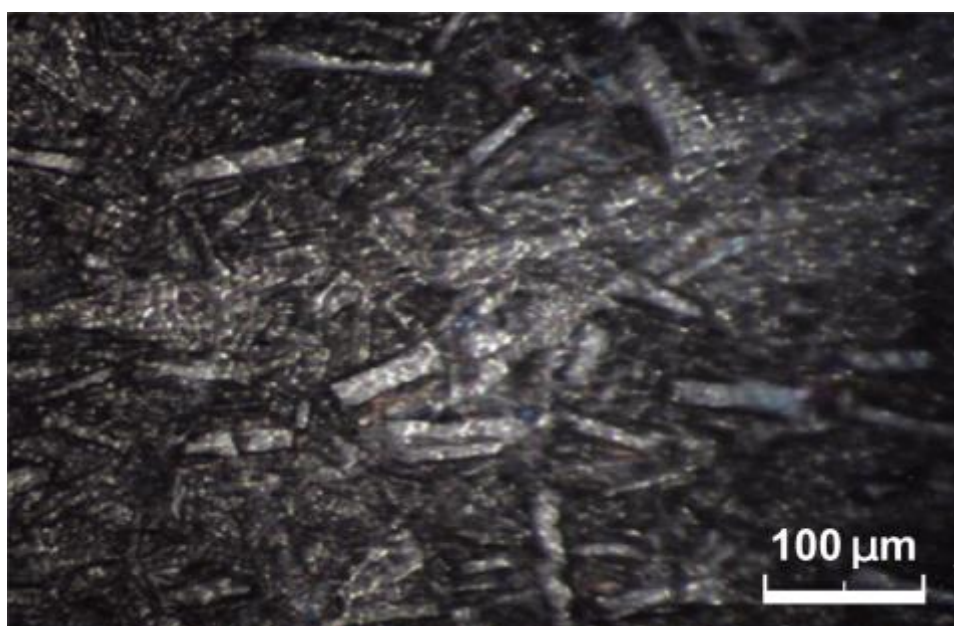


Figure 2.2: Optical microscope images of jute CNP taken with an H-C-Y Raman Microscope at a magnification of 10 times. This image depicts the inhomogeneity of the jute CNP topology with microfibers of varying dimensions.

In terms of mechanical properties, jute CNP was much weaker than pine CNP. Compared to the smooth and flexible nature of pine CNP, jute CNP felt rough and extremely brittle. When handling or cutting the jute CNP into desired sample sizes, even the slightest pressure from either one's hand or a blade would chip the nanopaper. In contrast, pine CNP has high measured flexibility and tensile strength of ~1 mm and ~60 MPa, respectively. It was difficult to obtain tensile strength measurements, as jute CNP would break from the tensile tester's sample clamps prior to testing.

The jute CNP's opaqueness and brittleness can be attributed to the inherently long and wide jute microfibrils. Since jute fibers have a diameter and length much larger than those of pine fibers, the TEMPO-oxidation process did not chemically break down the bleached jute pulp enough to yield an optimal homogeneous solution with nanoscale fibers. After mechanical treatment in the microfluidizer, the solution remained non-homogeneous. This phenomenon is visible in the microscope image in Figure 2.2, which displays that the jute fibers are of varying widths and lengths on the microscale. In comparison, the topology of pine CNP, found using **atomic force microscopy (AFM)**, can be seen in Figures 2.3 and 2.4. In these images, the pine fibrils are all geometrically similar, with dimensions on the nanoscale.

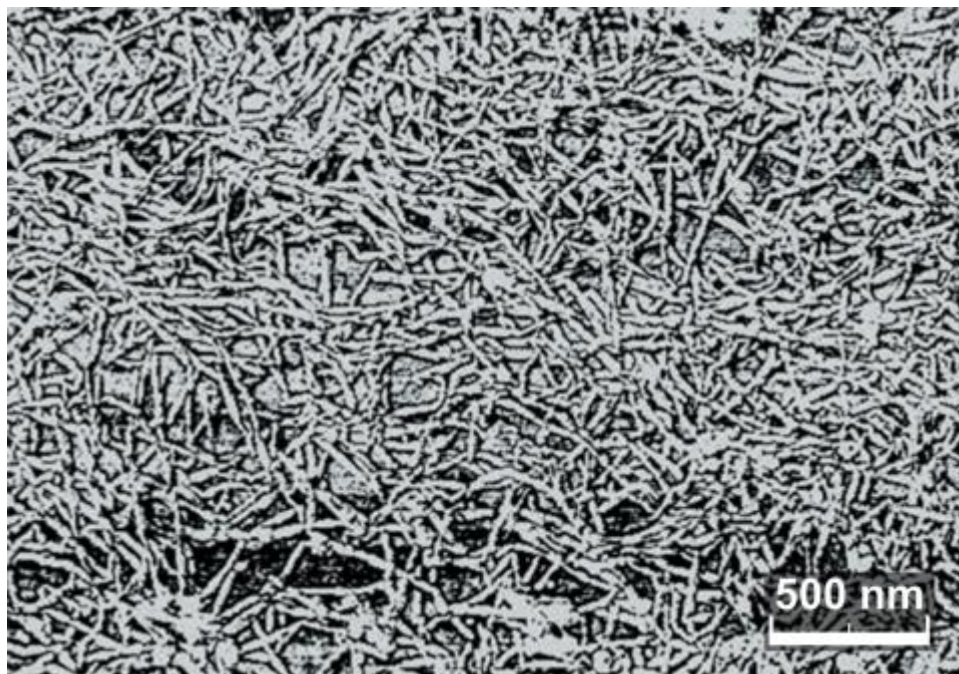


Figure 2.3: Atomic Force Microscopy (AFM) image of pine cellulose fibers taken with a D-3000 AFM machine, showing geometric and dimensional fiber uniformity.

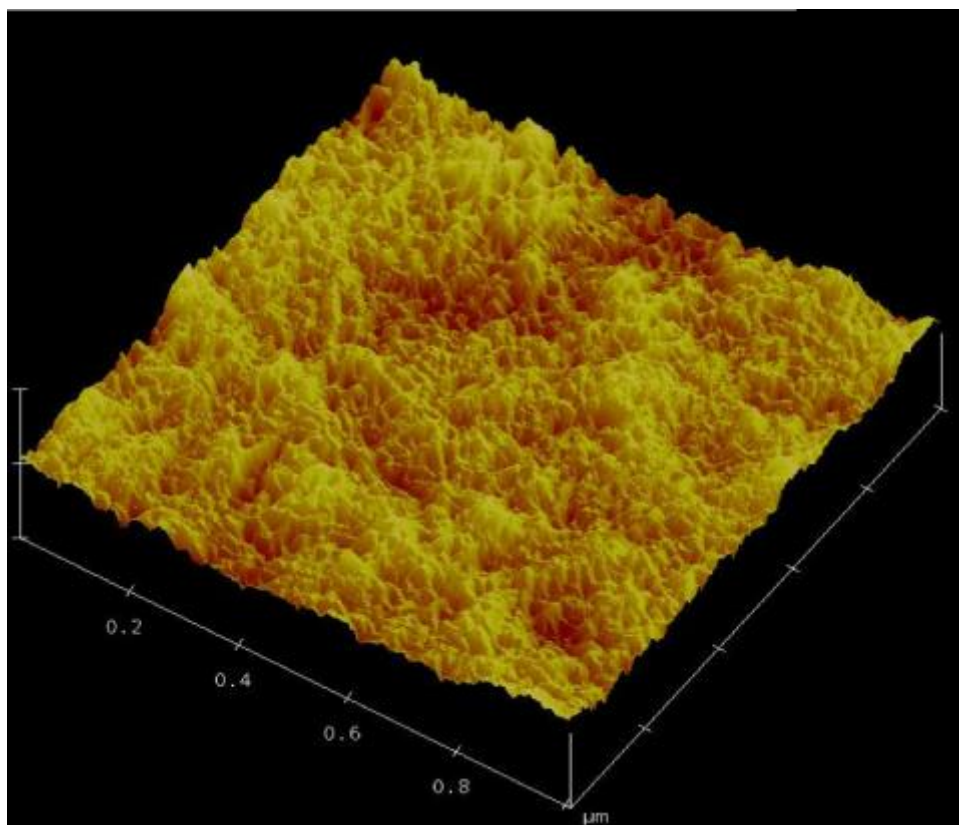


Figure 2.4: Three-dimensional AFM imagery of pine CNP displaying high density and porous topology.

The inhomogeneity of the jute slurry resulting from the TEMPO-oxidation process caused the clumping of cellulose fibers. During the drying process, the clumping of fibers allowed for areas in the casted solution to have greater mass and thus, uneven drying across the surface. The less massive areas dried faster than those with clumps, resulting in a brittle, curled CNP. Time in the humidity chamber could have been altered, but non-uniform drying would have persisted. The jute CNP had a packing density of a 1.10 g/cm³, while the pine CNP had a density of 1.24 g/cm³. Because of the non-homogeneous diameter of the fibers, the resulting jute CNP had a lower packing density than the pine CNP. This slightly lower packing density combined with clumping of fibers resulted in reduced strength and transparency of the jute CNP.

Moving forward, the TEMPO-oxidation process must be altered to accommodate for the long, wide jute cellulose fibers. Increased TEMPO-oxidation or multiple rounds of mechanical treatment are two viable alterations that would break down jute fibrils closer to the nanoscale, potentially resulting in a more transparent, flexible jute CNP. Moreover, further research should be conducted to investigate the relationship between the ratio of cellulose to hemicellulose and tensile strength. A diverse assortment of CNPs should be created from materials with varying chemical compositions. Another avenue to explore is the effect of a specific delignification process on the chemical composition of the resulting cellulose pulp. Fundamentally, the motivation for testing jute is to understand how a different composition of the cellulosic material affects the mechanical and optical properties of CNP, so a more rigorous approach must be taken to characterize the pulp before TEMPO oxidation.

Conclusion

After applying the manufacturing procedure of pine CNP to jute CNP, it was found that a jute CNP sample with improved mechanical properties and retained optimal transparency could not be achieved. Since the jute CNP was brittle, opaque, yellow in color, and nonhomogeneous in terms of geometry and fiber diameter, it was impossible to obtain measurements for tensile strength or transmittance. The evidence suggests that the increased brittleness is due to the longer and thicker fibers of jute cellulose.

Future Research

Jute cellulose remains a largely unexplored topic in the field of CNP. If the manufacturing procedure can be optimized to create a jute solution with more effectively broken down fibers, it is possible that jute CNP can have similar or even better properties than those of pine CNP. Hot pressing can also be explored instead of casting, as hot pressing is the traditional method of paper production and may produce a more densely-packed and homogeneous CNP. As a biodegradable and abundant material similar to pine, jute fiber holds promise as an eco-friendly starting material. When further developments are made to optimize its properties, jute CNP may have the capability to serve as a sustainable alternative material to plastics in electronic applications.

Chapter 3. Atomic Layer Deposition of Al₂O₃ to Improve Various Properties of Transparent Nanopaper

Abstract

Cellulose nanopaper (CNP) is a flexible, transparent, and renewable nanomaterial that is emerging as a replacement for plastics in various applications, including printed “green” electronics and thin films. Its remarkable strength (historically $\sigma \geq 200$ MPa), high transparency ($T = 90\%$) and flexibility (radius of curvature ≤ 3 mm) make it a promising material for the future. However, many of its potential applications require improvements in water stability, strength, and **functionality**. Atomic Layer Deposition (ALD) is a **conformal deposition method** that coats substrates through a two-stage process: the introduction of a metal-organic precursor followed by an oxidant. While ALD has been studied on cellulose **aerogels** and fibers on silicon substrates for various applications including oil separation from water, it has not been performed on CNP yet. In this study, use of ALD with aluminum oxide (Al₂O₃) on transparent nanopaper was demonstrated to increase insulating properties and functionality. Tensile testing was conducted to discern the effect of ALD on material parameters. This testing indicated an increase in the Young's modulus, which will be relevant for future device design, nanomanufacturing, and possibly replacing plastics in electronic applications.

Introduction

The structural integrity of CNP is crucial when considering its viability in harsh environments. Understanding the existing mechanical strength properties of nanopaper as a substrate is essential to optimizing it further for resistance to environmental factors such as wind, erosion, and other external forces. Relevant indicators of mechanical properties include tensile strength, **Young's modulus**, **strain-to-failure ratio**, and **bending radius**. Insufficient information on how to alter the microstructure of the material in terms of organization, alignment and coating to improve the values of these parameters has left a major gap in current research.

CNP has a highly porous, layered microstructure, which is unique among transparent substrates. The fibrous and porous layered structure gives the nanopaper excellent flexibility with a typical pore size between 10-50 nm, and also allows for release of stresses in the layers affected while bending an electronic device. This flexibility is a critical parameter in substrates when considering whether to use them in printable electronics. Additionally, it is easier to print on CNP than most other substrate materials due to its porous nature, which allows it to readily absorb ink (Zhu et al., 2014). CNP's flexibility has the potential to be improved by using malleable nanowires or nanotube films as the electrode materials and enhancing the device's structure so that the active **semiconductor** layer can be located close to the "**strain neutral**" (Huang et al., 2013). With improved flexibility, CNP could be used in applications such as flexible displays and sensors (Fujisaki et al., 2014).

However, higher flexibility has a direct relationship with larger pore size, which relates to lower tensile strength. Figure 3.1 provides **scanning electron microscopy (SEM)** imagery of the material showing a fracture surface.

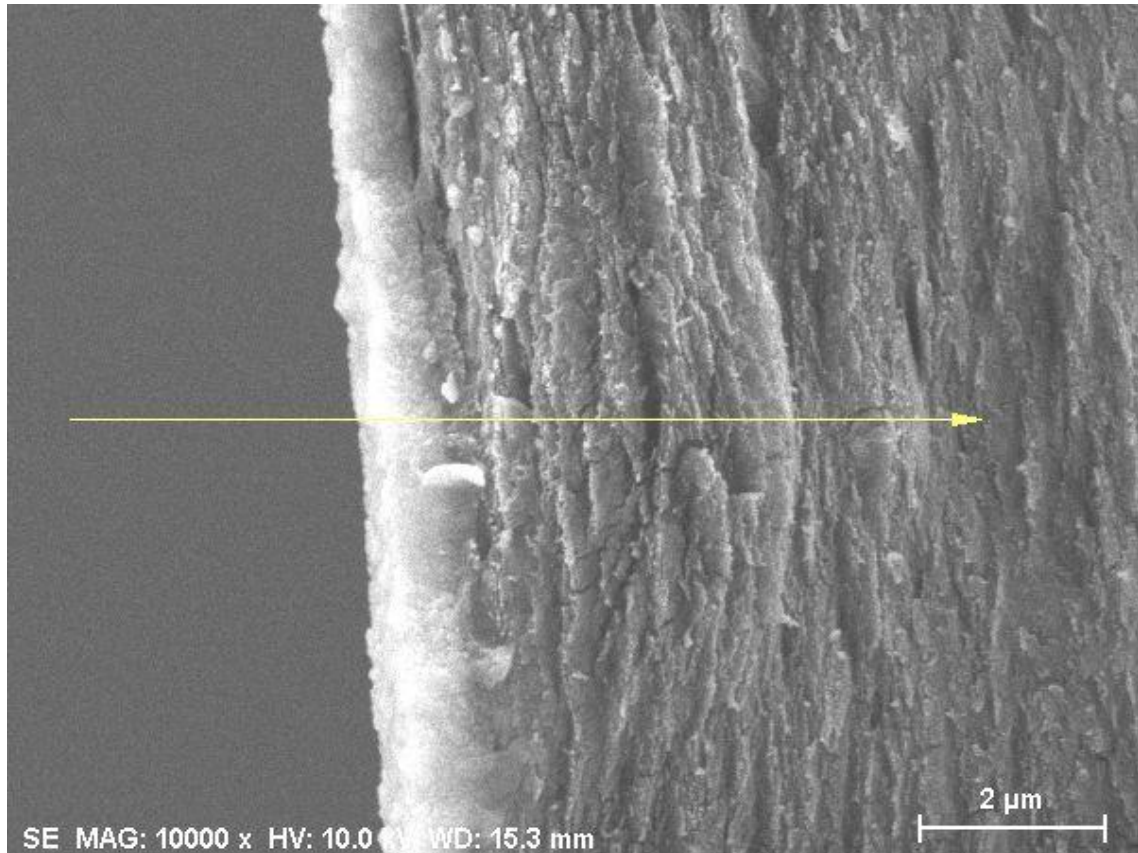


Figure 3.1: SEM image of a nanopaper cross section showing fiber structure on a fracture surface.

Current optimized CNP has a maximum tensile strength value of an impressive ~ 200 MPa occurring at 19% porosity (Zhu et al., 2014). This ratio of tensile strength and flexibility is ideal for roll-to-roll printing and 3D structure applications. However, despite these promising figures, the overall mechanical properties need to be improved further before CNP can be implemented in more robust applications. For CNP to remain competitive with plastic's tensile strength, its ultimate tensile strength must remain >60 MPa (Yu et al. 2014). Additionally, to be a

viable option for roll-to-roll processing, high flexibility must be persevered specifically a bending radius smaller than 1 cm.

Functionality. One proposed method of further improving the general functionality of CNP in electronic applications is Atomic Layer Deposition (ALD). ALD is a technique involving a sequence of chemical reactions that apply layers of thin films through deposition of vapors to a substrate, making it suitable for functional purposes, such as printed electronics (Banerjee et al., 2010). The basic model of the ALD reaction process is presented in Figure 3.2. These reactions use two precursors, which react with the surface of a material in an alternating, **self-limiting** manner; thus, a thin film is slowly deposited on the substrate (Banerjee et al., 2010).

The slow deposition rate of ALD reactions is unique to the process, facilitating precise uniformity of the films at an atomic level (Korhonen et al., 2011). An additional characteristic of ALD that makes it a unique deposition method is that it tends to run at lower temperatures than other forms of chemical vapor deposition (Korhonen et al., 2011). Ultimately, the deposited thin film enhances the substrate's surface conformability, thermal stability, and other physical properties that are crucial to its stability in an electronic setting (Groner et al., 2002).

ALD has steadily become more prominent within the last two decades as the respective sizes of electronic devices decrease and the **aspect ratios** in integrated circuits increase (Leskela et al., 2002). Many variations of ALD exist, involving differences in substrates and combinations of chemicals to facilitate different reactions. Most variations of ALD involve metal oxide precursors such as aluminum

oxide, zinc oxide, titanium dioxide, and zirconium dioxide, depending on the desired application (Leskela et al., 2002). Current substrates that are coated using ALD include gold, copper, cobalt, silicon, platinum, and more (Groner et al., 2002).

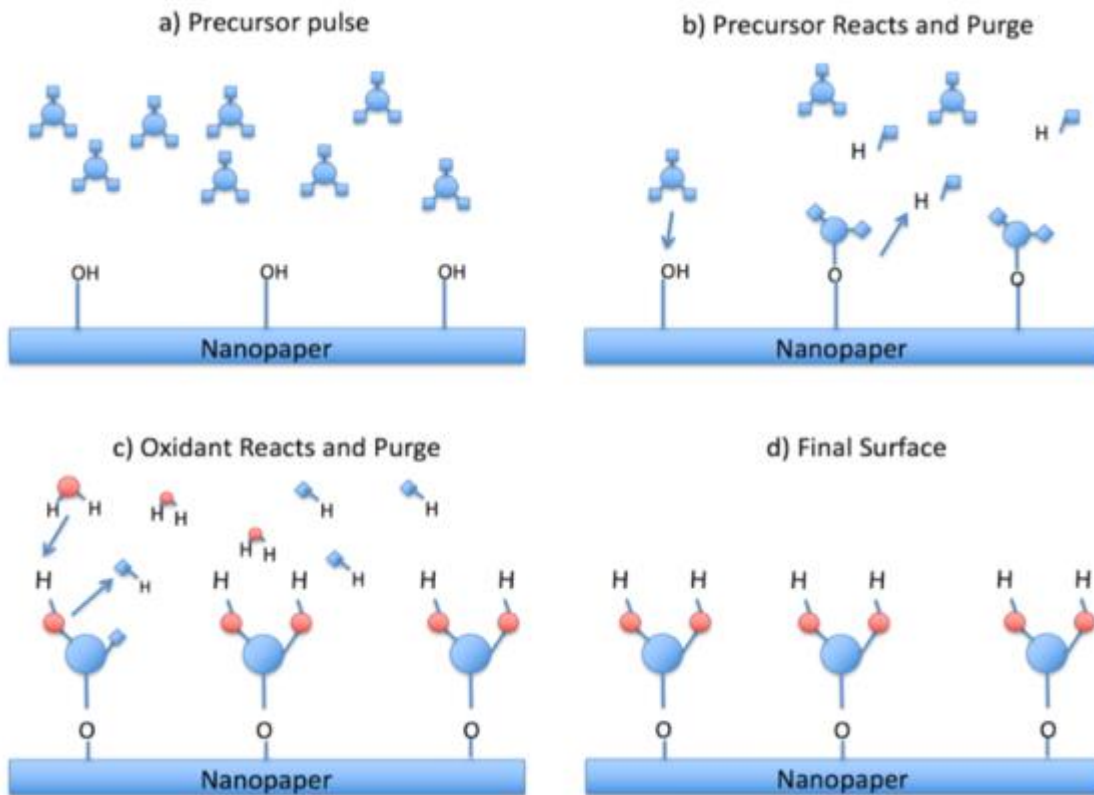


Figure 3.2: Schematic of the four stages of a basic model atomic layer deposition.

In a study at Aalto University in Finland, researchers performed ALD on nanofibrillated cellulose aerogels with aluminum oxide, zinc oxide, and titanium dioxide at 150 °C to prevent the decomposition of the cellulose. The authors demonstrated the efficiency of ALD by showing that the titanium dioxide-coated aerogels could act as humidity sensors, providing fast responses at 40 to 80 percent humidity (Korhonen et al., 2011). This study justifies cellulose as an appropriate substrate for depositing films through ALD, as it reacted with precursors effectively

and yielded the complete deposition of desired films. Based on the literature, it was assumed for this study that cellulose in the form of nanopaper rather than aerogels would also function effectively. Thus, this work investigates whether ALD can enable CNP to become viable in functional applications and renewable electronics.

Methodology

In this study, it was hypothesized that nanopaper will be a viable substrate for aluminum oxide (Al_2O_3) atomic layer deposition. Al_2O_3 ALD uses trimethylaluminum (TMA) and water as **precursor** materials (Banerjee et al., 2010). This method involved pulse cycles of distilled water and purge cycles of nitrogen gas (Elam & George, 2003). Appendix B contains reaction equations and process specifications for each method adapted this study.

A BenEq TFS 500 atomic layer deposition system was used to perform the depositions. Several samples were produced with a differing number of cycles (0, 250, 500 or 1000 cycles) to examine the differences between the amounts of material deposited. The 0-cycle sample was used to identify the effect of the baseline heat and pressure of the chamber on a control sample prior to the addition of the Al_2O_3 . Samples were also compared to standard pine CNP that remained at standard temperature and pressure.

The surface chemistry and morphology of CNP treated with ALD was then measured to determine the efficacy of ALD on CNP. Scanning electron microscopy (SEM) was used to characterize the surface of the Al_2O_3 coating with a beam of electrons.

Scanning Electron Microscopy. The films deposited by ALD were characterized by scanning electron microscopy to determine the growth rate of the alumina process and to characterize conformability and penetration of the film into the paper. Elemental dispersive x-ray spectroscopy (EDS) was used to determine film dimensions and penetration depth of the aluminum atoms. Additionally, it was hypothesized that cellulose may demonstrate multi-vapor phase infiltration (MPI) as demonstrated in spider silk by Eldridge et. al.

Tensile Testing. To find certain key properties of mechanical strength, such as elastic modulus, yield strength, failure stress, etc., a benchtop universal testing machine was used. A benchtop universal testing machine, such as the Tinius Olsen H25K-T benchtop universal testing machine (5,000 lb.), is a smaller version of a universal testing machine, which is used to measure the all-strength properties of larger wooden or metal members. The device output a stress-strain curve, from which necessary data was obtained for all 8 samples.

Flexibility. To determine the flexibility and foldability of the CNP samples, bending and folding tests were performed, respectively. For the bending test, metal rods of varying radii were used and the paper was folded around them. The objective was to find the rod with the smallest radius around which the paper could be folded before it broke or permanently creased, allowing for determination of the CNP's bending radius. For the folding test, processed CNP samples were folded and qualitative changes during and after the fold were assessed. Changes in general flexibility and any creases that were made in the CNP were also evaluated. Six samples were tested using each method.

Results and Discussion

SEM/EDS. Thickness of films deposited by ALD were characterized by SEM and shown in Figure 3.3 and Figure 3.4. The control sample exhibited no aluminum signal throughout the entirety of the sample, as expected. The sample with 250 cycles of ALD showed an aluminum signal corresponding to a thickness of 144 nm on the surface of the sample. The lack of aluminum signal in the bulk of the sample indicated that the precursor materials did not diffuse into the sample, despite the high porosity of the material. Additionally, there was no evidence of MPI in these areas. Finally, the 500-cycle sample exhibited a similar surface coating with a thickness of 180 nm.

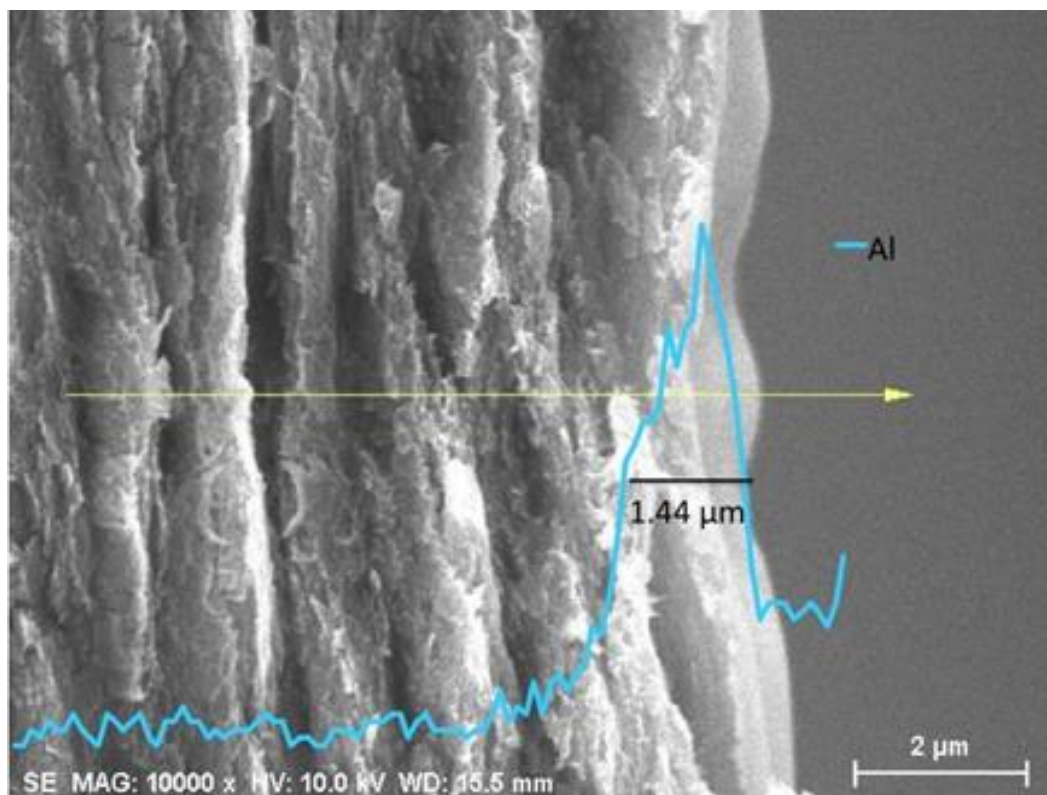


Figure 3.3: An SEM cross section of nanopaper treated with 250 cycles of Al₂O₃ showing a surface thickness of 144 nm.

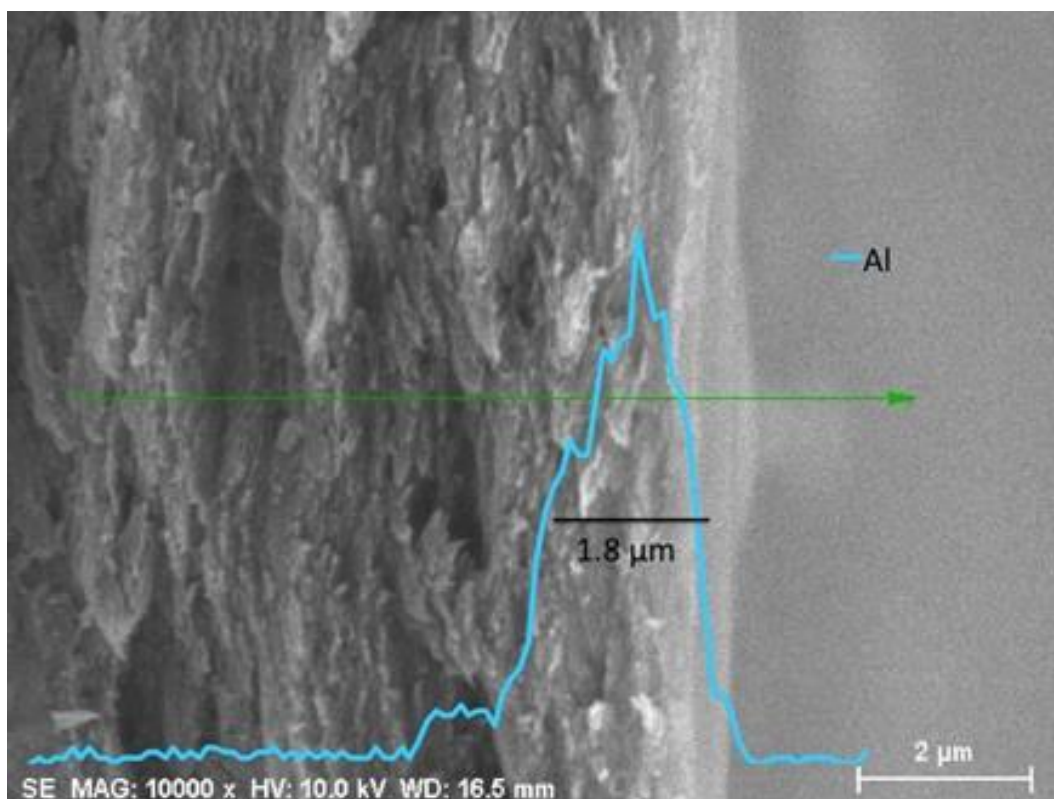


Figure 3.4: An SEM cross section of nanopaper treated with 500 cycles of Al₂O₃ showing a surface thickness of 180 nm.

Tensile Testing. A tensile tester was used to investigate how the Al₂O₃ ALD affected the mechanical strength of the cellulose nanopaper. It was determined that the process of ALD did not decrease the mechanical strength of the paper, consistently producing comparable results to standard pine cellulose nanopaper. Upon further investigation, it was concluded that the Young's modulus of the ALD treated samples improved compared to the standard pine cellulose nanopaper, as shown in Table 3.1. The results of the tensile testing are compared to each other on a stress-strain curve in Figure 3.5.

Table 3.1: Young's modulus of ALD and control CNP samples measured using a universal testing machine.

	Young's Modulus (MPa)	Ultimate Tensile Strength (MPa)
Untreated Pine	4.132	52.59
0 Cycles	3.773	46.86
250 Cycles	6.882	41.15
500 Cycles	6.953	51.56

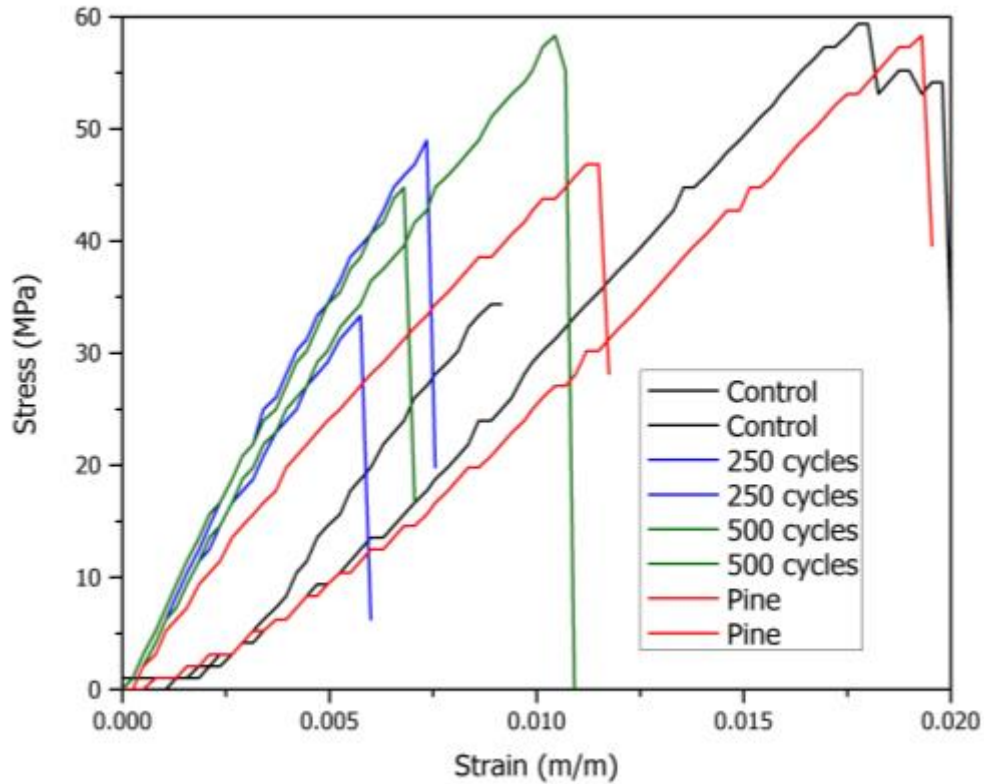


Figure 3.5: Comparison of stress-strain curves for ALD-treated and standard CNP samples.

Flexibility Testing. A commercially available bending and folding kit was used to determine the flexibility of the paper. The control, 250 cycles, and 500 cycle paper were all able to be rolled around the 1 mm radius without breaking or forming a permanent crease. For the folding test, each sample was folded and inspected for

damages. The control and 250 cycle samples broke along the crease; however, the 500-cycle sample did not break along the crease.

Conclusion

A successful deposition of ALD aluminum oxide (Al_2O_3) on transparent cellulose nanopaper created by casting was demonstrated in this study. The process exhibited a conformal coating on the surface of the paper. It was shown that for films of 125 nm to 250 nm, the ultimate tensile strength was unchanged. However, the Young's modulus increased with each successive ALD coating. These properties give a promising future direction to pursue for future device design, nanomanufacturing, and the possibility of replacing plastics in electronic applications.

Future Research

In terms of future research, SEM images suggested that cellulose nanopaper exhibits strong barrier properties for gasses, which prevents the ALD precursors from penetrating into the sample. At the relatively short pulse times (250 ms) and low temperature (120 °C) used in this process, the ALD alumina was deposited on the surface with minimal penetration and diffusion into the paper. Future research should fully investigate the penetration depth of the deposition as a function of pulse times, time after a pulse to allow for precursors to diffuse into the sample, and temperature. Additionally, further diffusion into the sample may demonstrate multi-vapor phase infiltration (MPI) as demonstrated in spider silk by Eldridge et al.

Chapter 4. Water Stability Improvements to Cellulose Nanopaper through Surface Reactions

Abstract

Cellulose nanopaper formed using TEMPO oxidation and mechanical shearing underwent two different surface-only treatments to increase the hydrophobicity of the paper. Half of the samples were treated with an esterification reaction using pivalic, benzoic, or octanoic acids along with a catalyst. **FTIR** data was collected for the different esterification samples. The remaining half of the samples underwent different numbers of cycles of atomic layer deposition (ALD) with aluminum oxide using a BenEq TFS 500 machine. Water contact angle and water weight change data were collected for each sample to evaluate hydrophobicity. Both tests indicated that ALD treatment slowed the uptake of water most effectively, while esterification showed smaller improvement over the control. Both sets of treated samples showed increased hydrophobicity over a 3-month period, although the effectiveness of the esterification treatment decreased over time. These improvements confirm that both treatments are viable in the short-term on TEMPO oxidized cellulose nanopaper, but further studies are needed to determine ways to prolong the effectiveness of esterification.

Introduction

To be a viable replacement to plastic in electronic applications, CNP needs to exhibit sufficient hydrophobicity due to the high likelihood of exposure to water in the environment. Cellulose is a highly **polar** material due to its many hydroxyl groups and thus will easily form hydrogen bonds with water. If exposed to water for an extended amount of time, the CNP fibers will dissociate and the paper will disintegrate, similar to printer paper. The ability to repel water without deformation is paramount in applications such as touch screens and solar cells. Because CNP is a highly porous material, water will soak through the pores in the paper. When the CNP absorbs water, its tensile strength drops by a factor of ten, which is unacceptable in potential applications (Sehaqui et al., 2014). Because of these issues with CNP, different methods of increasing its hydrophobicity were investigated to answer the research question: How can the hydrophobicity of CNP be enhanced while maintaining its biodegradability, and how will the resulting paper's water stability compare to that of plastics such as PET?

Several potential methods were discussed for altering the paper to improve its hydrophobicity. Ultimately, esterification and atomic layer deposition (ALD) were selected for use on the CNP substrate, as they are surface-only, environmentally friendly modifications that will leave the bulk material unchanged. Esterification involves a reaction between the alcohol groups on cellulose and organic acids, resulting in a hydrophobic ester group (Lee et al., 2011). A basic reaction is depicted in Figure 4.1; the mechanism for this study is indicated in Figure 4.2.

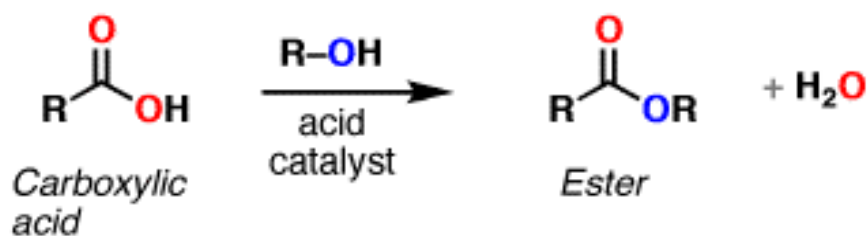


Figure 4.1: Generic carboxylic acid esterification reaction (Fisher & Speier, 1924).

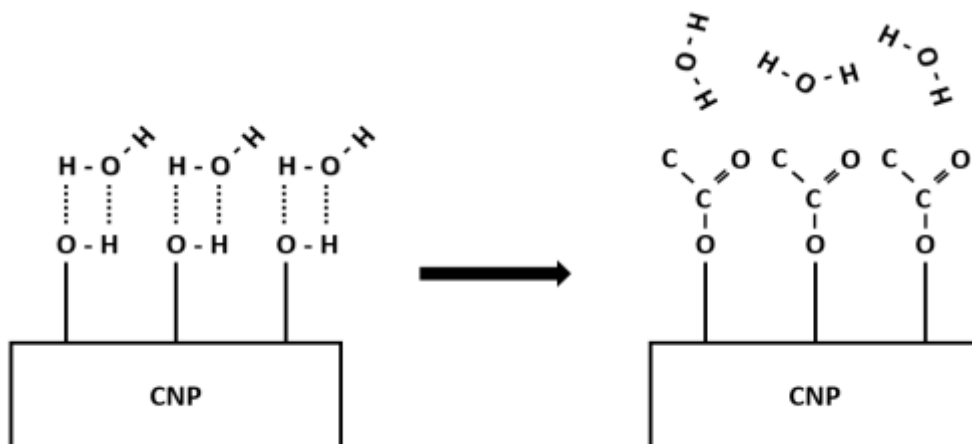


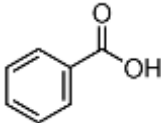
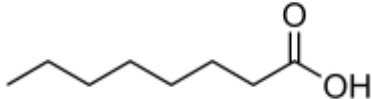
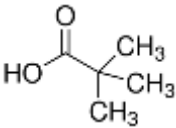
Figure 4.2: Reaction of alcohol groups on CNP to form hydrophobic ester groups.

Several research groups have performed similar research. Sehaqui et al. performed esterification on mechanically disintegrated cellulose fibers using organic acids and **anhydrides**, testing carbon chain grafts of 2, 4, 6, and 16 carbon atoms. Overall, their results showed that increasing carbon chain length reduced water uptake, increased contact angle, and increased tensile strength when wet. However, longer carbon chains also decreased dry tensile strength (Sehaqui et al., 2014). Lee et al. performed an esterification reaction on bacterial cellulose fibers using several organic acids and a p-Toluenesulfonyl chloride catalyst. The tested organic acids had chain lengths of 2, 6, and 12 carbons atoms. Similar to Sehaqui et al., their study found greatly increased water contact angles as the grafted chain length increased.

However, as the chain length increased, the thermal stability of the paper decreased rapidly (Lee et al., 2011).

Based on the findings of these groups, which treated the bulk material, this work has chosen to focus on benzoic, octanoic, and pivalic acids (Table 4.1) for a surface-only reaction. These acids, similar in size to side chains used in previous work, will allow for acquisition of a range of data to determine the effects of different organic acids on the properties of treated paper without encountering the issues of side chains which are too long. Several branch-chained acids were chosen to juxtapose results with the data from straight-chain alkane groups used in previous experiments. It was hypothesized that a surface-only reaction will similarly decrease water uptake while maintaining the paper's mechanical strength, thermal stability, and biodegradability, which are necessary for the aforementioned device applications. In this work, the simple esterification process presented by Lee et al. was applied on already-formed cellulose nanopaper formed by TEMPO oxidation and mechanical treatment.

Table 4.1: Organic acids used in esterification reaction.

Organic Acid	Structure
Benzoic Acid	
Octanoic Acid	
Pivalic Acid	

There are many different methods of characterizing a substance's interaction with water. Contact angle measurements, which are defined as the angle between a solid and liquid at a solid, liquid, and gas interface, quantify the **wettability** of the solid. Wettability is defined as the ability of a liquid to maintain contact with a solid surface due to intermolecular interactions. Qualitatively, larger contact angles result from less wettability and less surface interaction. Contact angle can also be calculated using the Young-Laplace equation (Equation 4.1) and the interfacial surface energies of the different materials.

$$\gamma_{SG} = \gamma_{SL} + \gamma_{LG} \cos \theta \quad (\text{Equation 4.1})$$

In this equation, γ_{SG} is the surface to gas interface energy, γ_{SL} is the surface to liquid interface energy, and γ_{LG} is the liquid to gas interface energy. Measuring

contact angle enables comparison of interfacial free energy between treated and untreated CNP.

Another simple test to determine changes in a substance's attraction to water is a weight change test, performed by submerging a material in water for a short amount of time. Materials with stronger interactions with water will swell and absorb more water than materials that are strongly hydrophobic. A weight change test determines the mass of water absorbed by a sample compared to its initial mass, allowing comparison between treatments designed to increase water stability. Qualitative data can also be gained by observing the consistency of CNP after removal to see how water has affected its structural stability.

The current material used in electronics is polyethylene terephthalate (PET), which exhibits contact angles of 72.5 degrees (Accu Dyne, 2017). PET exhibits 24-hour water absorption of 0.1% of its weight (Plastic Products, 2017). While it is not expected that PET's strong aversion water will be matched by CNP, similar short-term results may still be attainable.

Methodology

Experimental Procedure. This experiment was repeated three times with different organic acids: pivalic acid, benzoic acid, and octanoic acid. TEMPO-oxidized paper was obtained following the methodology detailed in previous chapters. Several strips of TEMPO-oxidized CNP were cut into approximately 5x1 cm pieces, weighed, and placed in a 1L round-bottom flask. Per gram of CNP, 200 mL of pyridine, 0.48 moles of organic acid, and 0.005 moles of p-toluenesulfonyl chloride were added. The round bottom flask was swirled to dissolve the organic acid,

then placed in a 50°C water bath under reflux. A stir bar was added to the mixture to ensure constant agitation while the reaction proceeded for 2 hours. Subsequently, the pyridine and excess reactants were removed, and the CNP was washed with ethanol and left to dry in ambient air in a Petri dish. For ALD samples, specimens treated using the parameters of the ALD process from the previous section were used.

Contact Angle. Measurements were taken for a sample of each esterification reaction after one day, three days, seven days, and 120 days following the reaction. On each day, a piece of the modified CNP was taped down to a flat surface. Two 10 μL drops were placed on each sample. Pictures were taken at a right angle to the drop at five-minute intervals for 15 minutes (0, 5, 10, and 15 minutes). The angle between the surface and droplet was found using a visual software GIMP with a built-in angle measurement tool as shown in Figure 4.3. Error in the measuring process was determined by taking five repeat measurements for certain randomly selected samples and calculating the standard deviation. The maximum deviation was found to be 3.5 degrees, which is assumed as the maximum possible error for all samples.

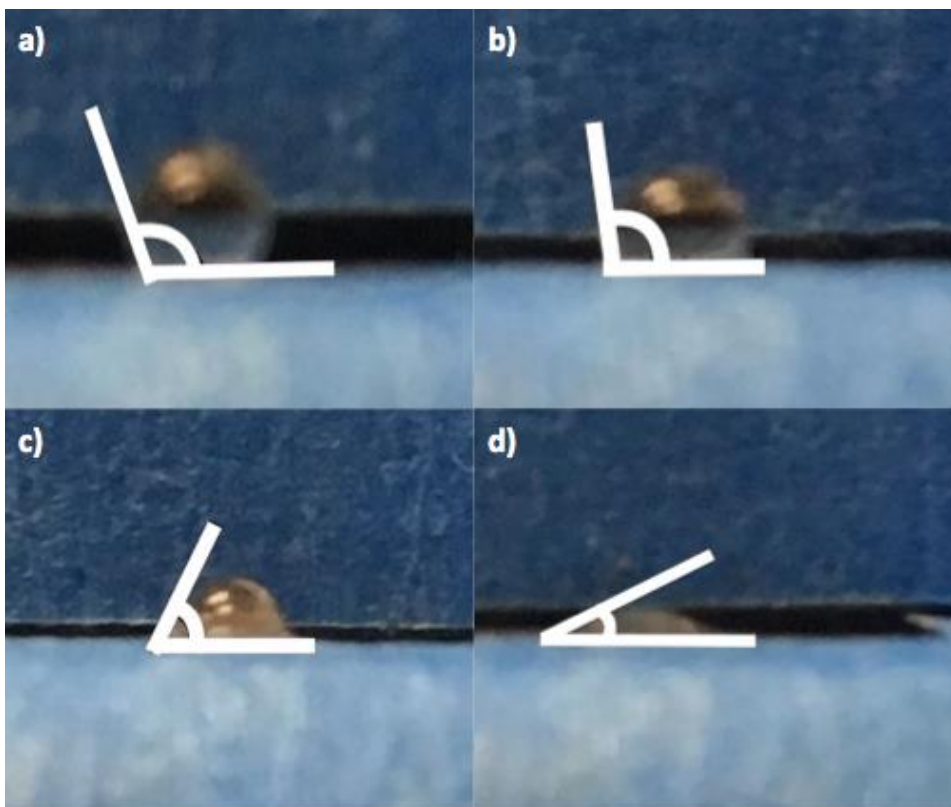


Figure 4.3: Contact angle measurements for CNP treated with 500 cycles of ALD at (a) 0, (b) 5, (c) 10, and (d) 15 minutes after droplet placement.

Weight Change Experiment. Absorption of water was measured using a weight change test. A sample from each treatment was weighed before being submerged in deionized water for 30 seconds. Samples were removed using tweezers, placed immediately on a tray, and weighed a second time. The percent change in weight of each sample was recorded. Error was estimated using the weight of a small droplet (assumed to be .01 g). This droplet represents water that could have been lost as the sample was transported from the solution to the measuring tray.

Fourier Transform Infrared Spectroscopy (FTIR). To identify the presence of functional groups of interest, **FTIR** was performed on untreated samples as well as those treated with the esterification process using a Thermo Nicolet

NEXUS 670 FTIR. The FTIR machine quantified the infrared percent transmittance of the thin films between 600 and 4000 cm^{-1} .

Results and Discussion

Weight Change. The absorption of water by the control sample and all six treated samples was measured. The weight change of each sample, given as a percent, is presented in Table 4.2. The percent was calculated as the mass of water absorbed (change in weight before and after submersion) as a percent of the starting mass of the paper. CNP treated with ALD absorbed the least amount of water relative to its size, followed by paper treated by esterification, with both treatments resulting in decreased water uptake compared to untreated CNP. In addition, the weight change of samples was grouped by treatment with all samples treated with ALD performing better than esterified samples. Because the weight change experiment was performed over a short period of time, it is applicable to the water diffusion rate of the samples as an indicator of water resistance. Therefore, water diffuses at a slower rate into samples treated with ALD, indicating increased water resistance compared to untreated CNP as well as CNP treated by esterification.

Among samples treated with ALD, those treated with 500 cycles had a slightly smaller weight change than did those that underwent 250 or 1000 cycles, displaying a greater water resistance at that optimized treatment level. A possible explanation for the decreased water resistance of ALD-1000 is its structural integrity; ALD-1000 paper was noticeably more brittle than ALD-250 and ALD-500, which could have allowed water to infiltrate the paper more quickly through small cracks.

Among samples treated with esterification, those treated with benzoic acid displayed the lowest percent change, followed by octanoic and pivalic acids.

Table 4.2: Water absorption as a percentage of mass of sample.

Sample	Percent Change	Error
Control	819%	± 76%
Octanoic	507%	± 60%
Pivalic	575%	± 42%
Benzoic	452%	± 35%
ALD-250	330%	± 18%
ALD-500	325%	± 17%
ALD-1000	360%	± 26%

Furthermore, it was observed that when exposed to water for extended periods, samples that had been esterified dissolved into solution well before control paper. ALD samples lasted the longest before completely losing their structure.

Contact Angle. The contact angles between water and treated and untreated CNP are shown in Figures 4.4-4.7. For each sample tested, the contact angle between water and the substrate decreased over the time the water droplet sat on the surface. This decrease was at a faster rate for untreated CNP than for either esterification or ALD samples. Untreated CNP's contact angle decreased by 40.2 degrees over the 15-minute time frame of measurement. The decrease for esterified samples ranged from 10.4 degrees (octanoic acid treated CNP) to 15.85 degrees (pivalic acid treated CNP). The effectiveness of the treatments over time was also assessed by measuring the contact angle a day after the reaction took place, a week later, and then 3 months

later. Between one day and one week, CNP treated with octanoic acid and benzoic acid experienced a slight decrease in the contact angle decrease over 15 minutes: 4.55 degrees for octanoic acid and 3.45 degrees for benzoic. CNP treated with pivalic acid experienced little to no change between the contact angle decrease over 7 days. Over 3 months, the contact angle decrease over 15 minutes increased dramatically: 34.1 degrees for octanoic acid, 33.1 degrees for pivalic acid, and 47 degrees for benzoic acid. The initial contact angle between water and treated CNP was similar 1 day after reaction and in the long term; however, the contact angle decreased more rapidly for older samples. This could mean that the treatment degraded over time.

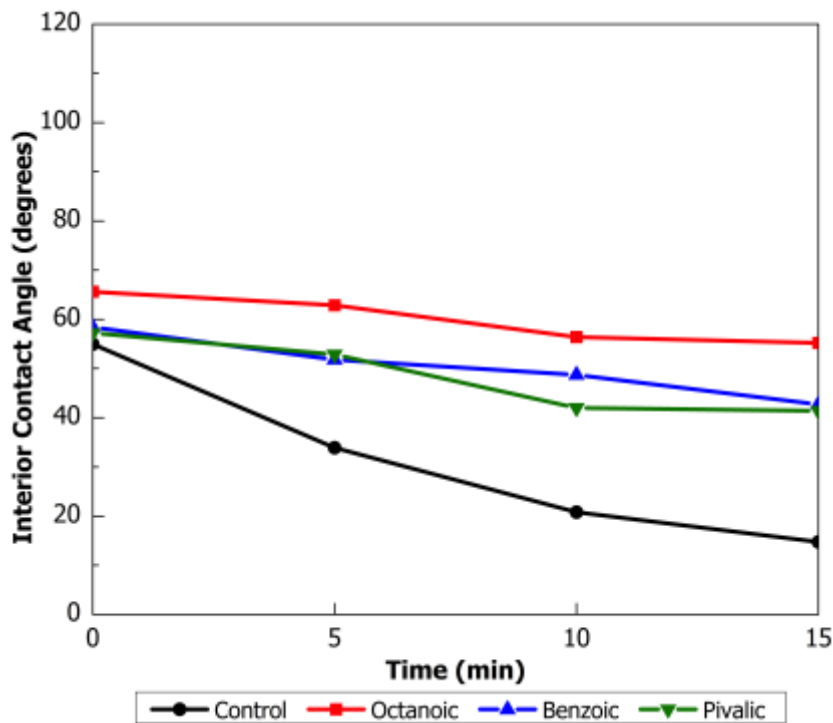


Figure 4.4: Contact angle between water, esterified, and untreated CNP over 15 minutes one day after reaction.

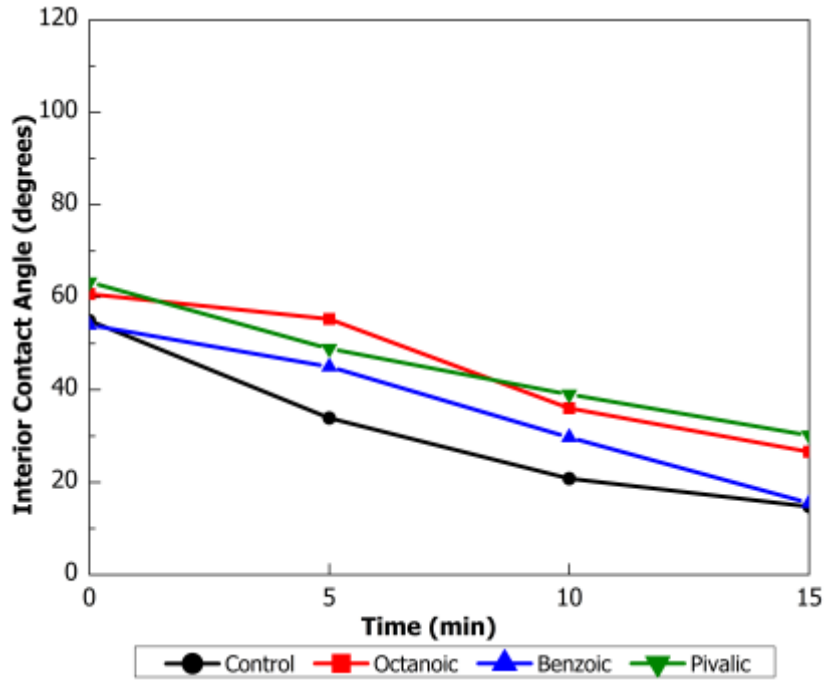


Figure 4.5: Contact angle between water, esterified, and untreated CNP over 15 minutes 120 days after reaction.

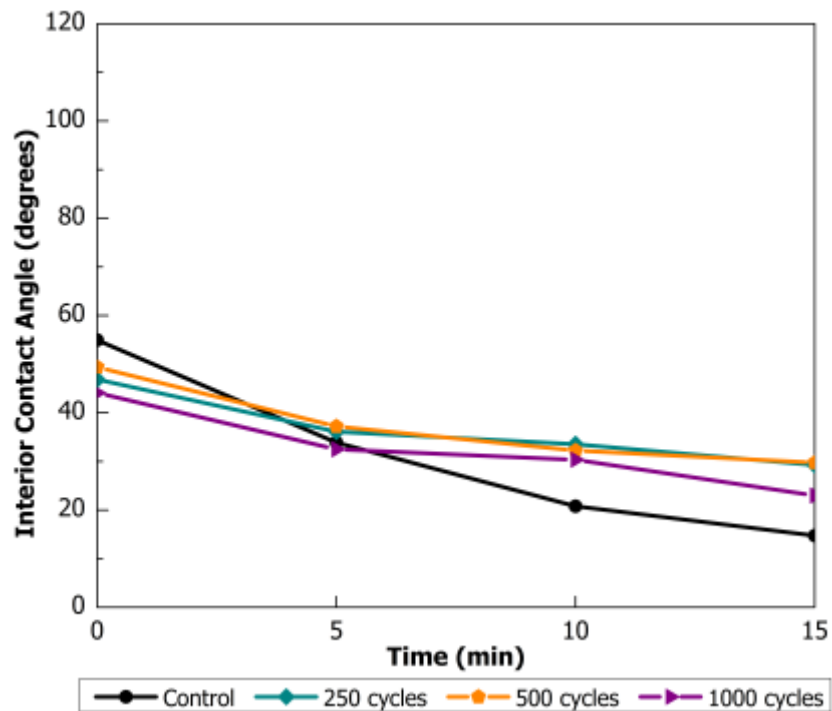


Figure 4.6: Contact angle between water, ALD treated, and untreated CNP over 15 minutes 1 day after reaction

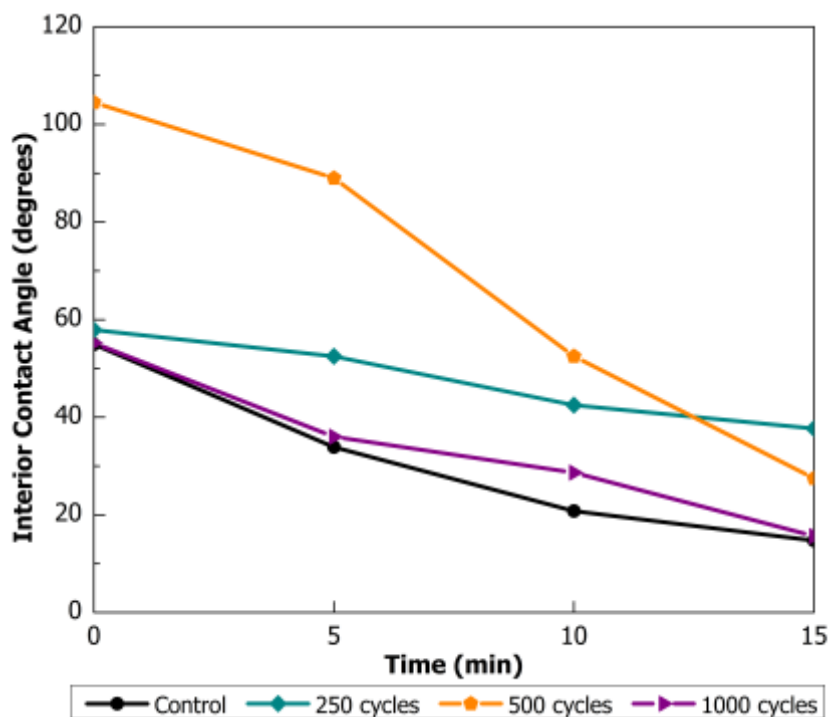


Figure 4.7: Contact angle between water, ALD treated, and untreated CNP over 15 minutes 120 days after reaction.

Initial measurements after water drops were placed were similar for esterification and control. As the water rested on the paper, the control sample's contact angle decreased rapidly, while esterified samples maintained the same contact angle. This is a result of the absorption of water into the material; the longer the drop rested on the CNP's surface, the smaller the contact angle became for all samples. However, the samples treated with esterification exhibited decreased absorption over 15 minutes, results which are corroborated by the weight change experiment.

ALD treatment and testing was performed multiple times with some issues with reproducibility. This is evident in the drastic differences between the short and long term ALD samples. These measurements were taken on different samples. The ALD tests after one day showed barely any increase over the control. However, another set of samples treated with ALD retained their hydrophobic properties well

over 120 days. The decrease in contact angle over 15 minutes was greatest for ALD-500, with a decrease of 77 degrees. This is compared to a decrease in contact angle of the untreated CNP of 40.2 degrees, ALD-250 of 20 degrees, and ALD-1000 of 39.5 degrees. The ALD-500 and ALD-250 samples retained a higher contact angle at the end of 15 minutes than did ALD-1000 and the untreated CNP. This large change in contact angle for ALD-500 is therefore likely due to its large contact angle at the time the water droplet was deposited; all other samples exhibited similar starting contact angles. The contact angle between ALD-500 and the water droplet was by far the largest of any samples tested, leading to the conclusion that, at least with an initial drop, ALD-500 exhibits the greatest hydrophobicity of methods tested when ALD treatment is successful.

Fourier Transform Infrared Spectroscopy (FTIR). Analysis of FTIR data (Figure 4.8) supplemented the observations described in the weight change and contact angle analysis of the samples treated with esterification. The samples of CNP treated with octanoic acid, which exhibited the highest hydrophobicity, also exhibited the largest decrease in FTIR peaks associated with hydrophilic alcohol groups compared to untreated paper. These samples also exhibited a slight increase in peaks associated with ester groups. The spectra of CNP treated with pivalic and benzoic acid were similar to that of the control, indicating that these reactions might not have been as effective as those with octanoic acid.

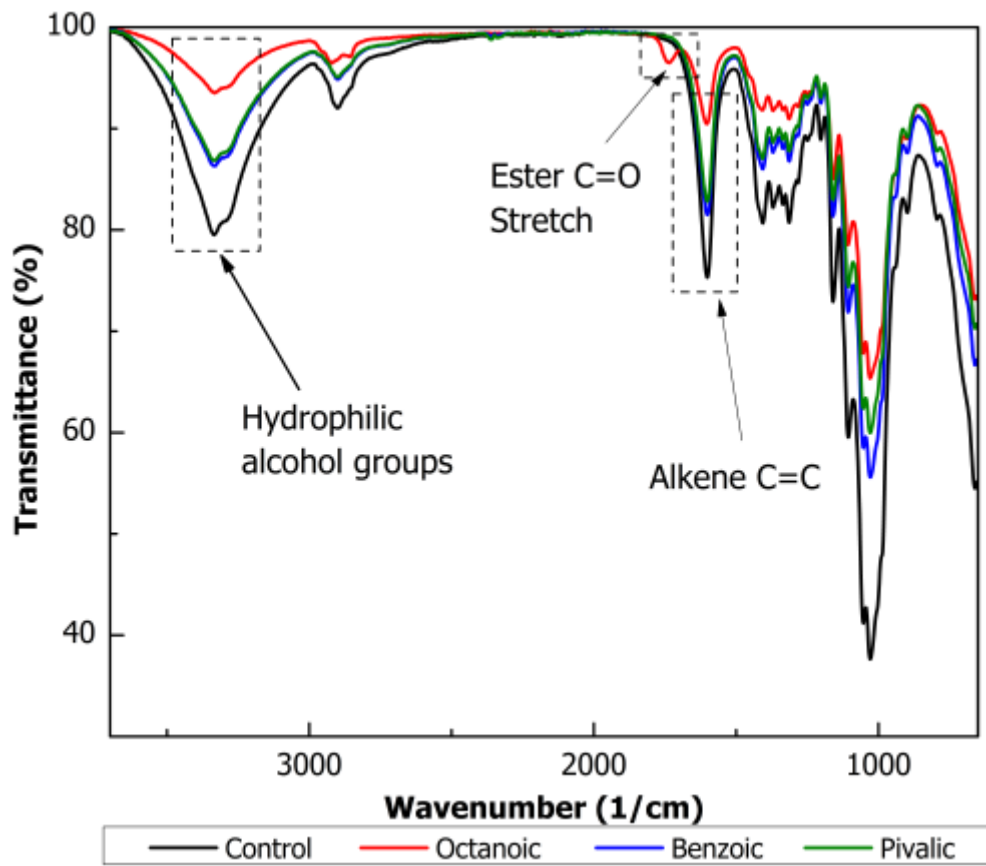


Figure 4.8: Combined FTIR Spectra of CNP treated with octanoic acid, benzoic acid, and pivalic acid with functional groups labeled. The emergence of a peak at ~ 1700 $1/\text{cm}$ indicates the emergence of an ester group.

Conclusion

Esterification treatment showed limited improvements in **surface free energy** as characterized by the contact angle test. This improvement was also evident in the weight change test. Water absorption into the substrate was slowed considerably compared to control, but not halted entirely. This is likely due to the porous structure of CNP. The surface-only esterification reaction did not completely seal the pores of the paper, which allowed water to seep in at a reduced rate. However, the esterification process did not change the chemical make up of CNP enough to alter its biodegradability, which is an important factor in a materials' sustainability. ALD

treatment showed increased improvement over esterification, but again did not halt water absorption. For use in full environmental conditions, this improvement is unsatisfactory and will not protect the paper. In certain limited environments, these treatments might provide increased performance and longevity. However, the in-depth manufacturing process for paper with these surface modifications will make them prohibitively expensive when compared to their performance. Compared to the water stability of PET, treated CNP still falls short, but the improvements made to contact angle and water absorption are important in the search for future methods of improving water stability without the use of plastics. Other solutions are likely viable which may improve the paper further while maintaining its eco-friendly quality.

Future Research

Based on these results, three recommendations can be provided in terms future research. First, it is important to gather more consistent data on ALD's effects on water stability. Some ALD exhibited the greatest hydrophobicity of all samples tested, while others were similar to control paper. Determining whether this was due to a process error or as a result of the ALD treatment itself will provide more insight into how effective ALD is overall at reducing water absorption by CNP. Second, degradation tests on all samples should be performed. With sustainability as one of the main goals of this project, it is critical to show that the treatments performed do not noticeably hinder the breakdown of the CNP after disposal. Likewise, the treatment must withstand degradation over time within most applications. Finally, the deposition of thin biodegradable plastic layers, such as polyhydroxybutyrate (PHB), should be investigated (Obeso et al. 2012). Due to the porous structure of CNP, it is

unlikely any treatment will fully repel water without completely sealing the surface of the paper. However, it is very probable that a very thin plastic layer will maintain the transmittance and strength of bulk CNP while preventing water from soaking into the paper.

Chapter 5. Scalable Carbon Nanotube/Cellulose Nanofiber Coatings on Cellulose Nanopaper and Derivatives

Abstract

In this work, a methodology for depositing conductive films on the surfaces of cellulose nanopaper and derivatives is reported to make them sufficiently conductive for flexible electronics applications. Derivatives included CNP with Al₂O₃ atomic layer deposition (ALD) of varying cycles and CNP esterified with pivalic acid. Two water-based conductive inks were developed, containing -COOH functionalized, **single-walled carbon nanotubes** (CNT) as well as one-dimensional (1D) cellulose nanofibers (CNF) as a sonicated suspension. 10:1 CNT/CNF ink was made with 10:1 w/w CNT/CNF and 2:1 CNT/CNF ink was made with 2:1 w/w CNT/CNF, with 5 mg/mL of CNT used for both inks. The inks were used to deposit thin, conductive CNT/CNF films onto CNP and its derivatives via a Meyer rod technique. Thicknesses of the films were measured to be 103.88 ± 1.376 nm from using 10:1 CNT/CNF and 104.16 ± 2.745 nm from using 2:1 CNT/CNF. **Sheet resistance** values as low as $62 \Omega\text{sq}^{-1}$ with transmittance of 36% at 550 nm were recorded, with nominal values varying with ink composition and CNP treatment type. The addition of CNF to the conductive inks resulted in increased transmittance and sheet resistance across all samples. Transmittance values were observed to decrease with a greater CNT/CNF w/w ratio. Through this experiment, conductive inks were modified to provide insight into producing coatings with desirable **conductivity** and optical transparency.

Introduction

Potential applications where CNP could replace plastics, such as touchscreens and printable electronics, demand that CNP exhibit electrically conductive properties. This poses a challenge, as CNP is a natural insulator. Previously, plastic substrates such as polyethylene terephthalate (PET) and polycarbonate had been coated to understand the mechanical performance and variations between inks comprised of CNTs and indium tin oxide (ITO). In a study conducted by Hecht et al., CNT films on PET were shown to have 86% total transmission (including the PET) and $600 \Omega\text{sq}^{-1}$. Through changes and improvements in tube purity, length, diameter, metal/semiconducting ratio, doping, formulation, and coating techniques, separate coatings of both 91% transmission and $500 \Omega\text{sq}^{-1}$ as well as 88% transmission and $250 \Omega\text{sq}^{-1}$ were achieved. A low total reflection of the CNT film on PET was also exhibited to be less than 5% across the visible spectrum, with most of the reflection due to the high reflection of the PET film itself. In contrast, ITO coatings on PET result in high reflection (which is undesirable), requiring the need for very expensive anti-reflective coatings (Hecht et al., 2009).

Attempts to make the surface of nanopaper conductive have produced conductive composite nanopaper, which utilize electrically active materials including **low-dimensional**, carbon-based materials integrated in the cellulose matrix (Feng et al., 2012, Imai et al. 2010). In addition, paper substrates have been shown to outperform plastics due to their ability to improve film adhesion, simplify the coating process and lowering costs significantly (Hu et al., 2009). Sheet resistance values of $10 \Omega\text{sq}^{-1}$ were obtained due to the conformal coating from the porous structure of the

paper. Large capillary force for the CNT ink was possible, which further enabled high contacting surface area between the CNTs and the paper after the solvent was absorbed (Hu et al., 2009). Recent studies using paper substrates have resulted in the fabrication of devices including flexible **transistors** (Fujisaki et al., 2014 & Huang et al., 2013) and **photovoltaic** devices (Zheng et al., 2013). PET, in contrast, resulted in significant film cracking and peel-off (Hu et al., 2009). Lastly, paper is far more sustainable than PET as thin plastic films can take up to thirty years to degrade (Zhu et al., 2013 [EES]) and consume limited natural resources like land and fossil fuels (Hopewell et al., 2009).

Hu et al. successfully deposited three separate conducting films of ITO, CNT, and silver nanowires (AgNW) on cellulose paper (2013). Standard printer paper, which was also coated with CNTs using a **Meyer rod** technique, demonstrated a sheet resistance of $10 \Omega\text{sq}^{-1}$ (Hu et al., 2009). In this work, CNT and AgNW films were deposited using an ink or suspension of the respective material. Meyer rod coatings are an effective choice because they are common in industry, suitable for scaling up to a roll-to-roll process, and can be applied to CNP as well as other substrates as demonstrated with printer paper (Hu et al., 2010). This coating methodology introduces novel aspects to utilizing CNP as a substrate, which demonstrates superior mechanical and optical properties as compared to printer paper and PET. For instance, CNP has been demonstrated to have a Young's modulus of 14.7 GPa (Henriksson et al., 2008) and transmittance (T_{diffuse}) of 90% at 550 nm (Hu et al., 2013).

In addition, when creating inks for conductive film deposition, it has been shown that adding **cellulose nanofibers (CNF)** may have desirable effects on the resulting ink. Hoeng et al. have shown that CNF may be added to inks as a **viscosity modifier** to not only increase uniformity of conductive coatings, but also act as a surfactant to help disperse the conductive material in the liquid. The efficacy of inks that include CNF as a viscosity modifier has been demonstrated on PET, but the same procedure on CNP has not yet been thoroughly investigated (Hoeng et al., 2016). Haijan et al. also recently utilized cellulose nanofibers to control the uniformity and transparency of CNT coatings. The authors detailed a scheme of interactions between cellulose nanofibers and carbon nanotubes that altered the surface charge between nanomaterials (Haijan et al., 2017). These interactions were employed in the subsequent methodology, in which hydrophobic-hydrophobic bonds between hydroxyl groups on the nanofibers and carboxyl groups on the functionalized nanotubes (Carbon Solutions, Inc.) bond together to produce a stable ink.

In this work, novel combinations of ink formulas and coating methodologies are deployed to optimize the electrical conductivity of CNP for device applications. This work investigates whether CNT/CNF films, deposited with the Meyer rod technique on a flexible, transparent CNP substrate, could exhibit a sheet resistance on the order of $10^2 \Omega\text{sq}^{-1}$ with at least 80% transmittance, which has not yet been observed in the literature. Although these methods of rendering CNP conductive were successful, the visible transmittances for nanopaper with ITO, CNT, and AgNW coatings were 65%, 60%, and 78% respectively, all of which were tested at 550 nm

(Hu et al., 2013). The methods to be discussed include controlling the ratio of CNTs to CNFs in a water-based ink. The CNFs act as a viscosity modifier and a **surfactant** to disperse the CNTs (Hoeng et al., 2016). Two different ink formulas were developed to investigate the effects of CNT/CNF weight ratio on visible transmittance and sheet resistance of samples coated with CNT/CNF films. In addition, to investigate how the substrate may influence the overall quality of the film, the conductive films were investigated on three different versions of CNP: CNP made with pine starting material, CNP with atomic layer deposition of Al₂O₃, and CNP treated with a pivalic acid esterification reaction. These methods resulted in films that demonstrated sheet resistances of 100 - 200 Ωsq⁻¹ as determined using a **van der Pauw** surface conductivity measurement and cross-sectional SEM analysis. Transmittance was measured across the visible and ultraviolet spectra from 400 nm < λ < 700 nm, and transmittance values at 550 nm were used for discussion. Finally, future methods for mechanical characterization are discussed.

Methodology

Table 5.1: Summary of cellulose nanopaper specimens coated with conductive ink for sheet resistance and transmittance determination. Two different inks were developed; Ink 1 had a nominal composition of 10:1 CNT/CNF w/w, while Ink 2 had a nominal composition of 2:1 CNT:CNF w/w. Two samples of each type listed were coated, e.g. one per ink.

CNP Sample ID	Cellulose Source	Surface Treatment	Description
C1, C2	Yellow pine	None	Control specimen
A11, A12	Yellow pine	250 cycles of Al ₂ O ₃	Atomic layer deposition
A21, A22	Yellow pine	500 cycles of Al ₂ O ₃	Atomic layer deposition
A31, A32	Yellow pine	1000 cycles of Al ₂ O ₃	Atomic layer deposition
E1, E2	Yellow pine	Esterified via pivalic acid	Surface reaction to increase hydrophobicity

Note: For samples on which atomic layer deposition (ALD) was performed, the first number in the sample ID denotes the number of reaction cycles, and the second number in the sample ID denotes which ink was used for coating. For all other samples, the number denotes which ink was used for coating. For instance, A12 refers to CNP with 250 cycles of ALD coated with Ink 2, and C1 refers to untreated CNP coated with Ink 1.

Nanopaper Preparation. Huang et al. previously optimized a unique method for CNP development and fabrication (Huang et al., 2013). This procedure involves first deriving cellulose nanofibers (CNF) from wood pulp through a disintegration process, which is possible due to the hierarchical structure of wood fibers. Through iterative mechanical and chemical processes, CNFs with diameters ranging from 5-60 nm are obtained (Zhu et al., 2014). Historically, CNFs have been extracted from several naturally occurring sources of cellulose before being processed into CNP. It should be noted that all samples in this work, unless otherwise specified, were reduced from Kraft bleached softwood pulp derived from southern yellow pine. A procedure adapted from (Huang et al., 2013) was employed wherein 78 mg of 2,2,6,6-Tetramethylpiperidine-1-oxyl (TEMPO) and 514 mg of NaBr were first

combined with 5g dry weight of pulp in 50 mL deionized water. TEMPO-mediated oxidation of the fibers commenced when 30 mL of 12 wt% NaClO was added to the suspension at room temperature and agitated at approximately 300 rpm. The pH of the reaction was closely monitored and small aliquots of 12 wt% NaOH were added every 15 min for 2h to maintain a pH of 10.5. Then the residual TEMPO was removed from the reaction product by **Buchner funnel** filtration, in which the fibers were rinsed using distilled water until a cake of fibers was obtained. Next, the fibers were added to distilled water at a 1 wt% concentration and sheared via high-pressure homogenization using a Microfluidizer M-110EH (Microfluids Ind., USA), yielding a cellulose nanofiber suspension. Subsequently, **sonication** was performed on the nanocellulose suspension before the filtration process was repeated, in preparation for casting. Finally, the fiber solution was casted on a smooth surface in a Constant Temperature and Humidity Chamber (Chincan Model LHS-150HC-11), and allowed to dry over several days at controlled humidity of 50-60% until the sheet of nanopaper could be removed.

Carbon Nanotube Ink Fabrication. Inks were prepared using -COOH functionalized single-walled CNTs from Carbon Solutions (P3-SWNT) as well as CNF, which acted as a surfactant and viscosity modifier. For the first ink, CNF suspension was combined with 50 mg -COOH functionalized CNT in deionized water to obtain a proportion of 50 mg CNTs to 5 mg CNFs (10:1 w/w). The ink with this CNT/CNF ratio is henceforth referred to as *10:1 CNT/CNF*. 10:1 CNT/CNF was bath sonicated for 5 minutes, after which it was probe sonicated for 5 minutes with a 500

W, 20 kHz probe at 30% amplitude. Second, functionalized CNTs and CNFs were again dispersed in water; however, here the target proportion was 50 mg CNTs to 25 mg CNFs (2:1 w/w). This suspension is henceforth referred to as *2:1 CNT/CNF*. The same process was followed above with **bath sonication** followed by **probe sonication**. Both inks were derived from the same 1.34 wt% solution of CNFs to prevent discrepancies in composition and to yield a concentration of 5 mg CNT/mL. The inks were allowed to stabilize overnight to ensure uniform suspension, shown by Figure 5.1(a). Inks were used within one week of preparation to ensure CNT stability in the suspension. A full experimental procedure is reported in Appendix C.

Meyer Rod Ink Deposition. The ink deposition process is depicted in Figure 5.1. A flat surface was covered with a fresh sheet of aluminum foil and thoroughly cleaned with ethanol before each CNP specimen was anchored to the foil. A #12 Meyer rod was used to apply the coatings and was cleaned thoroughly between trials. Prior to deposition of the ink, CNP specimens were mechanically pressed for 24 hr. to ensure a flat, even surface. Similarly, both inks were bath sonicated for another 5 minutes before coating to ensure even distribution of the CNTs and CNFs within the ink. For each coating, 100 μ L of dispersed ink was deposited above the top edge of the CNP with a micropipette, displayed by Figure 5.1(c). The Meyer rod was quickly drawn over the ink toward the user and over the substrate with uniform pressure along the rolling direction (RD in Figure 5.1). All CNP specimens listed in Table 5.1 were coated using this same procedure. For more details on the coated specimens, information can be found in the previous chapters on atomic layer deposition of

Al₂O₃ and esterification reaction with pivalic acid. Each film was allowed to dry for at least 20 min before the specimens were detached and mechanically pressed for 24 hr., to prevent deformation and to lower the junction resistance before characterization.

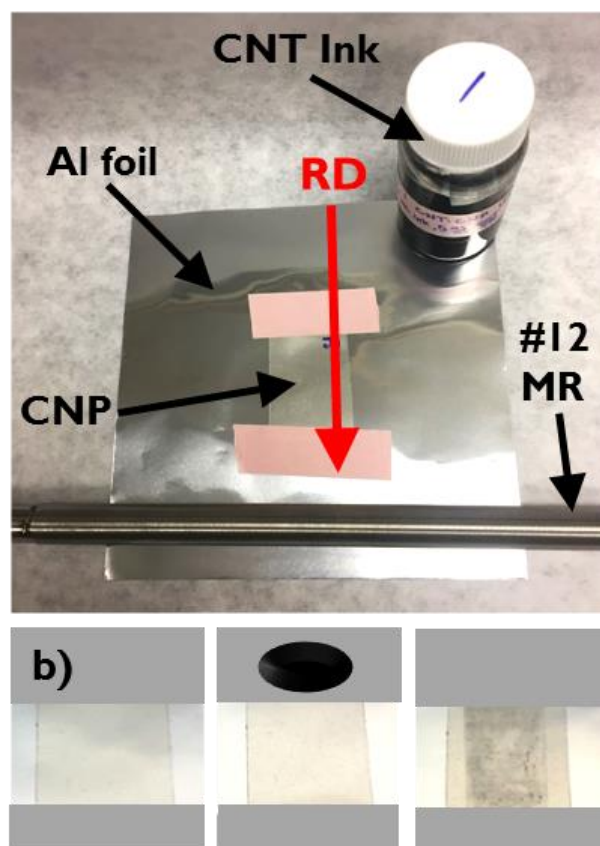


Figure 5.1: Fabrication and coating of CNT ink (a) Configuration of conductive ink and CNP rolling setup with #12 Meyer rod (MR) pulled down and towards the user across the CNP surface. (b) CNP sample before, during, and after coating with conductive ink.

Conductive Film Thickness Determination. Cross-sectional SEM (Tescan XEIA FEG SEM) was performed in secondary electron imaging mode to measure the conductive film thickness. Samples consisted of two coated pieces of untreated CNP, one with 10:1 CNT/CNF and the other with 2:1 CNT/CNF. To prepare cross-sectioned samples, coated CNP samples were stored in a freezer at -18°C for 24 hr.

and then broken into pieces to expose cross-sections of the conductive-coated region. Before imaging, the samples were coated with a thin layer of gold to ameliorate charging effects. The resulting cross-sections are shown in Figure 5.2. The thickness of the conductive film for each inks was determined to be 103.88 ± 1.376 nm for 10:1 CNT/CNF and 104.16 ± 2.745 nm for 2:1 CNT/CNF.

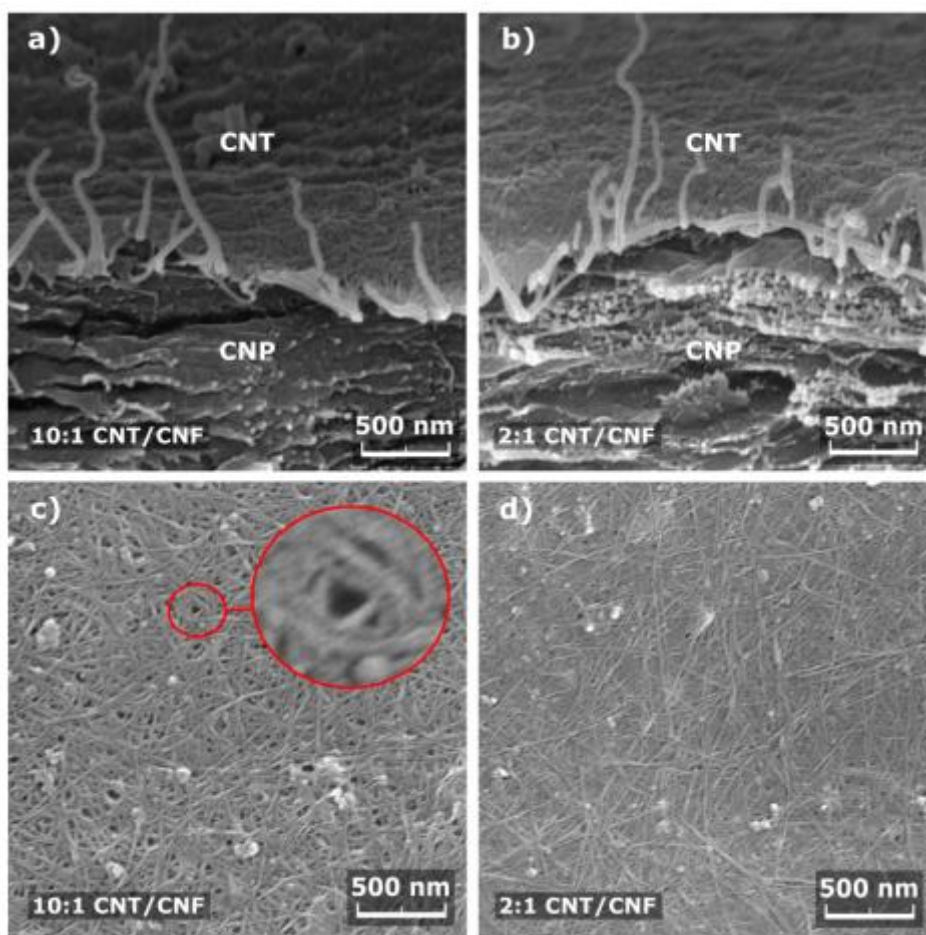


Figure 5.2: Secondary electron images taken with a Tescan XEIA FEG SEM. (a) and (b) display cross-sections of cellulose nanopaper samples C1 and C2 coated with 10:1 and 2:1 w/w CNT/CNF respectively. The film thicknesses were measured to be 103.88 ± 1.376 nm for 10:1 CNT/CNF and 104.16 ± 2.745 nm for 2:1 CNT/CNF. Panels (c) and (d): top-down views of hot-pressed conductive films rolled using the 10:1 and 2:1 w/w CNT/CNF inks respectively. Inset in the 10:1 coating shows negative space, where there are larger and more numerous holes in the 10:1 film than in the 2:1 film. This leads to lower transmittance.

Sheet Resistance Determination. Sheet resistance measurements were derived from cross-sectional film thickness determination detailed subsequently and conductivity measurements obtained using a HMS-5000 **Hall Effect** Measurement system (Ecopia Corp). After coating, 1 cm x 1 cm coated samples were attached to a sample board anchored to the lid of a 0.55 T magnet chamber using 4 spring-loaded connectors as shown in Figure 5.3(a). The conductivity of the film was then found using the van der Pauw technique (Thurber, 2008). An automated system measured the voltage between points A and B V_{ab} , as well as V_{bc} , V_{ac} , V_{cd} , V_{da} , V_{bd} while reversing current before calculating conductivity for each specimen at room temperature. Subsequently, conductivity measurements were converted to sheet resistance values, presented in Figure 5.3(b), using a film thickness of 103.88 ± 1.376 nm for 10:1 CNT/CNF and 104.16 ± 2.745 nm for 2:1 CNT/CNF as determined from Figure 5.2.

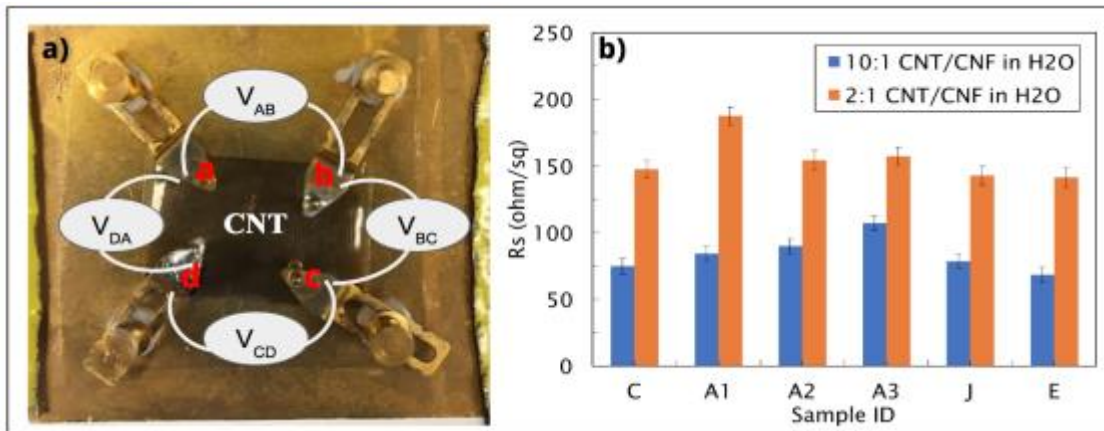


Figure 5.3: Experimental setup of (a) Hall effect characterization of carbon nanotube (CNT) coatings on cellulose nanopaper (CNP). Hall voltage coefficients measured across pins a, b, c, d were used to calculate (b) average sheet resistance, R_s , of conductive films.

Optical Transmittance Determination. A Perkin-Elmer Lambda 25 UV/Vis spectrophotometer was used to measure the transmittance of all samples for $200 \text{ nm} < \lambda < 700 \text{ nm}$. After a 100% transmittance calibration trial, data was recorded within this range and the 550 nm value was selected for discussion. The 550 nm value corresponds to the maximal human eye sensitivity and is thus commonly used for transparency measurements (Hoeng et al., 2016). The resulting values were analyzed for discrepancies between samples with different combinations of treatments and ink formulas.

Results and Discussion

SEM (Tescan XEIA FEG SEM) was used in **secondary electron** imaging mode to investigate the rod-coated CNT/CNF films whose cross-sections are shown in Figure 5.2 (a) and (b). From these images, the thicknesses of the films rolled using 10:1 CNT/CNF and 2:1 CNT/CNF were determined to be $103.88 \pm 1.376 \text{ nm}$ and $104.16 \pm 2.745 \text{ nm}$, respectively. The film thicknesses were calculated as weighted averages where the uncertainty on a single measurement was assumed to follow a Gaussian distribution. Figure 5.4 depicts the relative thickness of the CNT film as compared to the CNP substrate, which was determined to have a thickness of 82 microns.

The top-down views of the conductive films in Figure 5.2 display the hot-pressed nature of the coatings. **Hot pressing** was performed for 24 hr. shortly after rolling to reduce the junction resistance, the primary contributing factor to resistance in carbon nanotube networks (Hu et al., 2010). SEM shows the size of voids ("holes"

of negative space in the coatings) in conductive networks rolled using 10:1 CNT/CNF to be ~ 90 nm for $75 \Omega\text{sq}^{-1}$ films. The void size can pose a problem if it is larger than the charge diffusion length, and can be reduced by increasing the density of nanotubes (Hu et al., 2010). The void size in films rolled using 2:1 CNT/CNF is smaller at ~ 40 nm, where the CNFs partially fill in the holes and reduce their size. The filling of voids by CNFs is not linked to a contribution to electrical conductivity, but is associated with reduced scattering of light by negative space in the films. This thereby increases the transparency of the material to incident radiation.

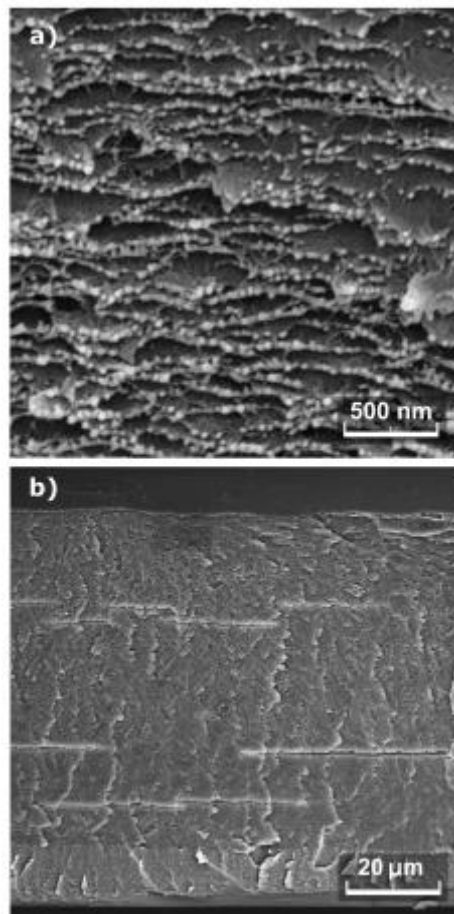


Figure 5.4: Secondary electron images of (a) cross-section of the CNP substrate with visible nanostructure, and (b) entire cross-section of the coated CNP substrate, taken with a Tescan XEIA FEG SEM. Diameters of cellulose nanofiber bundles in (a) range from 25 - 40 nm.

Figure 5.3 shows sheet resistance values for samples used in the experiments, which include standard CNP, CNP coated with Al_2O_3 via ALD, and CNP esterified using pivalic acid. The sheet resistances of films prepared with 10:1 CNT/CNF were lower in each case than for 2:1 CNT/CNF. Thus, contrary to what was found by Hoeng et al., it was found here that the addition of a greater amount of CNF to the CNT ink detrimentally affected the sheet resistance of the conductive networks, sometimes by over a factor of two. This could be attributed to the different ink preparation procedures used here and by Hoeng et al. in 2016. The only sample to show an improved sheet resistance over the untreated CNP was the esterified CNP. Films on other treated samples had higher resistance relative to the control CNP, and more investigation is necessary into why this is the case.

Figure 5.5 displays transmittance spectra for all samples used in the experiment. For all six samples, the substrates naturally have higher transmittance than their CNT/CNF coated counterparts. Similarly, Figure 5.5 shows that films prepared using 2:1 CNT/CNF outperformed films prepared using 10:1 CNT/CNF in terms of transmittance. This is consistent with the smaller and fewer number of holes found in the 2:1 CNT:CNT films compared to the 10:1 films, which serves to reduce the amount of light scattered while incident radiation passing through.

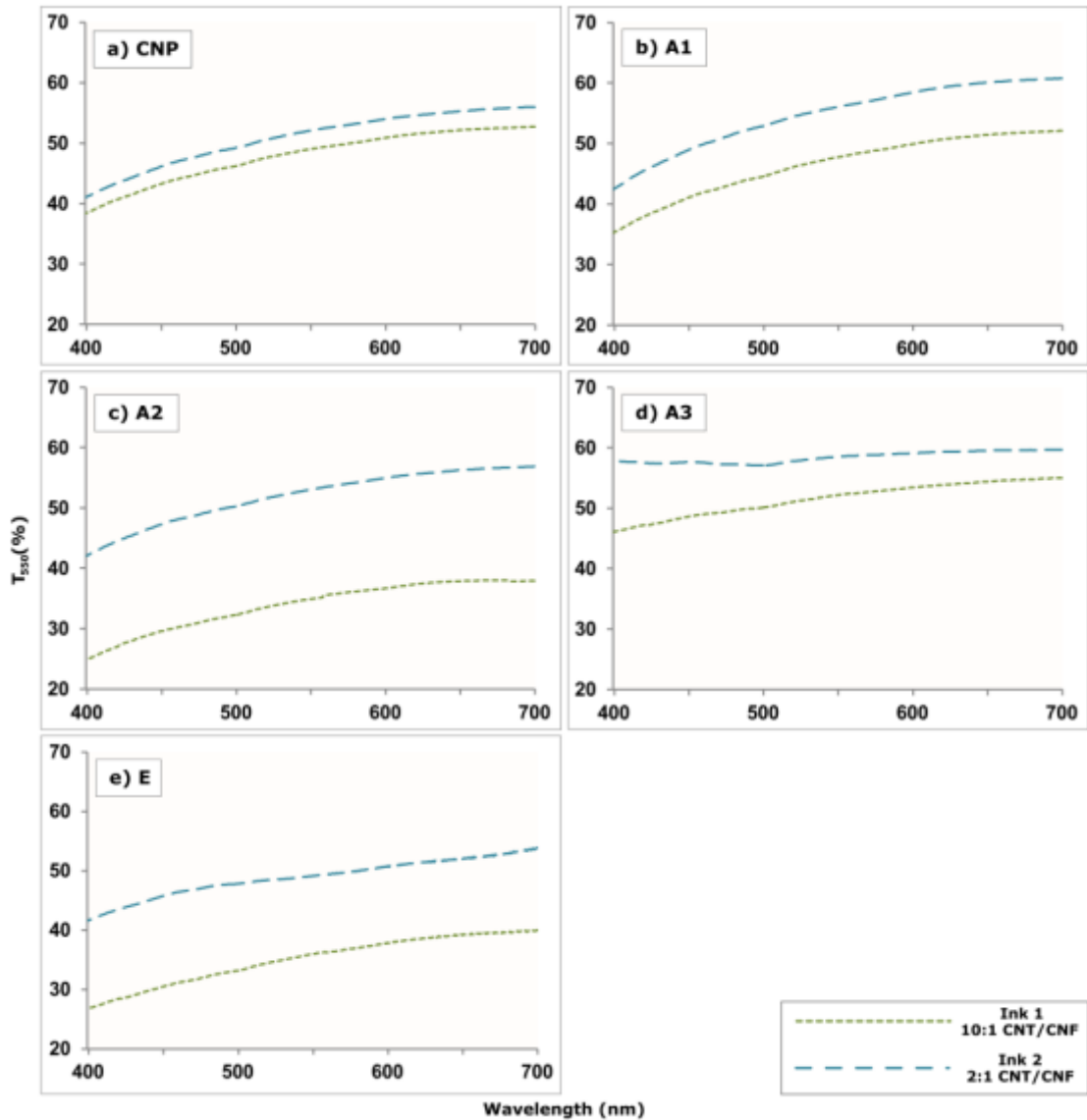


Figure 5.5: Transmittance measurements for all sample types: (a) C, (b) A1, (c) A2, (d) A3, and (e) E. Through all samples, 10:1 CNT/CNF coatings exhibited lower transmittance than those of 2:1 CNT/CNF, in line with the findings that a larger proportion of CNT/CNF would result in this phenomenon.

As a benchmark, all transmittance data will be described at 550 nm. Figure 5.6 displays the sheet resistance and transmittance for each sample in a way that highlights the relationship between the two properties. The data reflect that a desirable, lower sheet resistance comes with lower optical transmittance. Looking at the extremes, sample A32 exhibited the highest transmittance at 58.55%, while

sample A21 had the lowest at 34.89%. A12 had the highest sheet resistance (208.42 Ωsq^{-1}) while E1 had the lowest sheet resistance (62.06 Ωsq^{-1}). It is also interesting to note that E1 and E2, the CNP samples esterified using pivalic acid, outperformed A21 respectively in terms of their placements in Figure 5.6. Exhibiting the lowest sheet resistances of all treated specimens, E1 and E2 also exhibited higher transmittance than A21. Therefore, Figure 5.6 indicates that 10:1 CNT/CNF outperformed 2:1 CNT/CNF in terms of sheet resistance, but 2:1 CNT/CNF outperformed 10:1 CNT/CNF in terms of higher transmittance. Statistical analysis was subsequently used to verify this hypothesis.

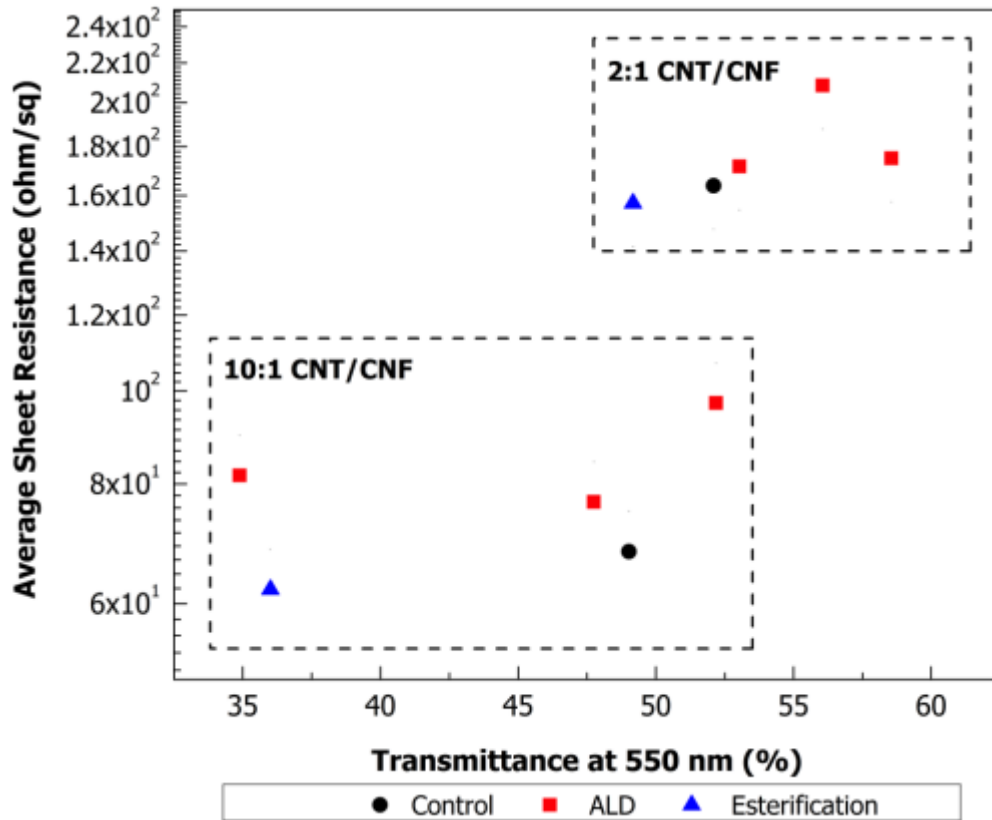


Figure 5.6: Sheet resistance and transmittance for all samples separated by inks. There exists an apparent and logical tradeoff between sheet resistance (Ωsq^{-1}) and % transmittance. A higher CNT/CNF concentration results in a lower transmittance as well as a lower sheet resistance.

To determine whether the variation in the transmittance and sheet resistance of the conductive films as a result of varying the CNT/CNF ratio was significant, a paired t-test was used. The statistical tests carried out for each performance metric (sheet resistance and conductivity) as indicated in Tables 5.2 and 5.3 allow us to draw conclusions about the difference of the true means for each ink formula. In both cases, the null hypothesis was a mean difference of zero, meaning that there was no significant difference in the sheet resistance or transparency for the two formulas. The claim that the true difference exceeds zero was tested by calculating a T-statistic, T , and calculating the probability that this value was less than or equal to the true difference, t , given that the null is correct. P-values of 0.0002038 and 0.01036 were calculated for sheet resistance and transmittance, respectively. At a fixed significance of 0.05, there is sufficient evidence to reject the null for each performance metric to 95% confidence.

Table 5.2: Paired T-test: Difference of Means (Sheet Resistance)

	10:1 CNT/CNF	2:1 CNT/CNF
Mean (Ωsq^{-1})	77.10	175.2
Variance (Ωsq^{-1})	183.0	393.9
Observations	5	5
Pearson Correlation	0.3156	--
Hypothesized Mean Difference (H_0)	0	--
Degrees of Freedom (n-1)	4	--
P($T \leq t$) one-sided	0.0002038	--

Table 5.3: Paired T-test: Difference of Means (Transmittance)

	10:1 CNT/CNF	2:1 CNT/CNF
Mean (Ωsq^{-1})	43.97	53.78
Variance (Ωsq^{-1})	63.31	13.14
Observations	5	5
Pearson Correlation	0.7173	--
Hypothesized Mean Difference (H_0)	0	--
Degrees of Freedom (n-1)	4	--
P($T \leq t$) one-sided	0.01036	--

From these results, there exists a clear tradeoff between sheet resistance and transmittance; the lower the sheet resistance, the lower the transmittance. With a higher CNT/CNF concentration in 10:1 CNT/CNF, it is expected that these inks would be less transparent and more conductive, yielding a lower sheet resistance. However, it is ultimately more important for the samples to have a lower sheet resistance for electronic application purposes. Furthermore, esterified CNP was the only sample to outperform untreated CNP in terms of sheet resistance for both inks. These findings may be attributed to the slight increase in hydrophobicity of CNP, which occurs because of the surface esterification reaction with pivalic acid. Ongoing work indicates this may forestall sample deformation when exposed to water-based solutions (such as the ink formulas utilized here).

Potential errors affecting the accuracy of sample characterization include the difficulty of measuring the exact transmittance of all samples due to varying degrees of inhomogeneity of the coatings. Variations in the applied pressure with the Meyer rods along the rolling direction may have contributed to this error. Therefore, when

measuring the visible transparency spectra of the samples, there is a range of possible percentages for each wavelength that could have been achieved depending on where on the sample the beam is hitting and the ink coating composition and thickness at that point. Taking multiple spectra at different locations for each sample and observing the variation in transmittance values would help to account for this error. There could have been errors in terms of the angle at which the beam hit the samples due to the curvature of the coated samples. This error may be reduced by producing samples which are more flat and easily mounted in the spectrophotometer sample holder, which can likely be done with a modified mechanical pressing procedure.

Fibrous materials such as CNTs show promise as conductive coating materials on CNP. Hu et al. coated CNP with CNT with results of $R_s=200 \Omega\text{sq}^{-1}$ and $T_{\text{diffuse}}=60\%$ (Hu et al., 2013). A novel ink fabrication and coating method was presented here that yielded optimal results of $R_s = 62.06 \Omega\text{sq}^{-1}$, $T_{550} = 36.00\%$ (E1, 10:1 CNT/CNF) and $R_s = 208.42 \Omega\text{sq}^{-1}$, $T_{550}=56.06\%$ (A12, 2:1 CNT/CNF). By improving the sheet resistance and lowering it to a range from 62.06 through 208.42 Ωsq^{-1} , the results suggest the possibility to optimize CNT/CNF compositions of the inks further, for films with lower sheet resistance and higher transmittance to use in various flexible transistors and photovoltaic devices. Further additives need to be explored to prevent the agglomeration of CNTs, which hinders charge carrier transfer between individual nanotubes and thus lowers the overall sheet resistance. For instance, the ability of various "wrapping polymers" as well as surfactants to suspend

and de-bundle single-walled CNTs has previously been investigated (Haggenmueller et al., 2008).

Ideally, the transmittance at 550 nm needs to be increased by a factor of 2 to allow adequate light penetration for photovoltaic applications. However, these results still advance understanding of methods to lower the sheet resistance of CNT coatings by an order of magnitude, producing results comparable to AgNW coatings (Zhu et al., 2014). This would increase the performance of the flexible devices in development. To develop results discussed here further, future work on the mechanical robustness of the CNT/CNF films through tests such as bending radius and **mechanical film adhesion** will be investigated. Models for these tests have been established already in literature (Hu et al., 2013 & Hoeng et al., 2016).

Environmental/Health Effects. It should also be noted that the environmental effects of the combined treatments and toxicology could not be investigated in the project timeframe; these interactions with living organisms present a critical consideration for future device iterations. The small diameter of engineered nanomaterials such as carbon nanotubes may reduce the volume footprint of waste from the aforementioned CNT/CNP products. However, water-soluble fullerenes and carbon nanotubes are likely to be scaled up in the future, resulting in unnatural concentrations of nanomaterials in groundwater and soil, providing an impetus for further study of the environmental risks associated with nanotechnologies (Colvin, 2003). Additionally, Pulskamp et al. found that commercially produced dimensional carbon materials incubated with mammalian cells produced an increase in

intracellular reactive oxygen species as well as a decrease in mitochondrial membrane potential. While the authors emphasize that no acute toxicity was observed and the effects on cell function are not yet understood, these effects must be researched further before large-scale implementation of CNT/CNP in household devices (Pulskamp et al, 2007).

Conclusion

In this work, cellulose nanopaper and its derivatives coated with novel formulas of conductive films have exhibited moderate sheet resistance and optical transparency. Paper substrates have been proven to outperform plastics, both in terms of their functionality when coated with CNT-based inks as well as their implications for sustainability. The porous structure of the paper aided the CNT ink to exhibit large capillary force and high contacting surface area between the CNTs and paper. Two inks containing -COOH functionalized single-walled CNTs were fabricated to investigate the relative composition of conductive additives and viscosity modifiers, and were deposited with a Meyer rod technique. The use of cellulose nanopaper and its derivatives showed how various surface treatments in conjunction with conductive coatings yield optimal results ranging from 62 - 208 Ωsq^{-1} and 35 - 58% transmittance at 550 nm.

Future Research

These findings indicate new avenues for depositing conductive, transparent films on CNP, an insulating and fibrous material, by altering the proportion of

conductive material to viscosity modifiers, with CNF being used as a novel surfactant in the CNT/CNP product. Future work would include investigating the mechanical adhesion of the conductive films on the CNP, and the flexibility of the conductive films as a function of film composition. Mechanical adhesion of the films to the CNP substrate could be compared with adhesion to current plastics as a quantitative metric. Knowledge in these areas would provide a more complete characterization of the films as well as begin to test mechanical criteria for their use in electronics.

Chapter 6. Conclusion

This work demonstrates that CNP is a promising candidate to replace plastics in optoelectronics and flexible electronics. It is already highly transparent, mechanically robust, flexible and thin, inexpensive to fabricate, and biodegradable. As shown by the four treatments to CNP, properties such as the water stability, electrical conductivity, and mechanical strength can be modified to fill in shortcomings where the performance of plastics, like PET, currently exceeds that of CNP. Thus, CNP may replace plastics while performing at the same operating standards. Touch screens, solar cells, batteries, and flexible transistors are all extremely common devices in the society of today and are applications where the uses of CNP have begun to be realized. If plastics can be phased out in favor of CNP, nonrenewable sources used to manufacture and dispose of plastics can be preserved, and a more sustainable, future-oriented approach to electronics can be realized.

This thesis has discussed four research processes to enhance selected properties of CNP. In the first, the starting material was changed from softwood pine pulp to jute to investigate the resulting altered mechanical strength, optical properties, and flexibility. Modifications such as enhanced mechanical strength were expected because of the relatively longer molecular chains of cellulose found in jute fibers. The existing pine CNP manufacturing procedure was used on jute fibers with the result that jute CNP was brittle, non-homogeneous, opaque, and yellow in color. Furthermore, the jute CNP was unfit for property testing such as mechanical strength and optical transparency due to the brittleness and inhomogeneity of the material. Jute cellulose remains a largely unexplored topic in the field of CNP, and thus there are

many directions this research can be taken. A methodology that breaks down jute fibers more effectively could result in CNP that has properties similar or better than that of pine CNP. Additionally, hot pressing can be explored as a method instead of casting, as hot pressing is the traditional method of paper production, and therefore may produce a more homogeneous CNP. Although this method of fabricating jute CNP production was unsuccessful, additional methods should be investigated in further research.

In the ALD treatment process, Al_2O_3 was deposited on CNP to investigate properties of the altered material. The process exhibited a reasonable growth rate of 5 nm/cycle and conformal coating on the surface of the paper. ALD was shown to increase insulating properties and functionality. For films of 125 nm to 250 nm thickness, the bending radius and tensile strength of CNP were unchanged. However, the Young's modulus increased with ALD coating. These properties give a promising future direction to pursue for future device design and nano-manufacturing. The maintenance of high tensile strength and low bending radius qualify ALD as a potential treatment for CNP in future competition with plastics in electronic applications. In terms of future research, SEM images suggested that CNP exhibits strong barrier properties for gases that prevent the ALD precursors from penetrating into the sample. At the relatively short pulse times (250 ms) and low temperature (120 °C) used in this process, the ALD alumina was deposited on the surface with minimal penetration and diffusion into the paper. Future research is needed to investigate the penetration depth of the deposition as a function of pulse times and temperature. Additionally, further diffusion into the sample may demonstrate multi-

vapor phase infiltration (MPI) as demonstrated in prior literature (Eldridge et. al., 2012).

The third research process consisted of performing two different surface-only reactions on CNP to increase its hydrophobicity. Half of the samples were treated with an esterification reaction using one of pivalic, benzoic, or octanoic acids and a catalyst. The other half of the samples underwent different number of cycles of Al₂O₃ atomic layer deposition as previously discussed. Water contact angle and water weight change data were collected for each sample. Both tests indicated ALD treatment slowed the uptake of water most significantly while esterification showed smaller improvement over the control. Both sets of treated samples showed increased hydrophobicity over a three-month period, although the effectiveness of the esterification treatment decreased over time. ALD and esterification exhibited maximum water contact angles of 105 degrees and 68 degrees, respectively, which decreased steadily over time. While the common electronic plastic PET exhibits a contact angle of 72.5 degrees, which did not decrease over time, the aforementioned treatments showed an increase of as much as 55 degrees with respect to untreated CNP. Additionally, ALD and esterification decreased the water absorption of CNP by 58% and 38%, respectively. While this decrease is an improvement, it is still marginal with respect to PET, which has a 24-hour water absorption of as low as 0.1% of its weight (Plastic Products, 2017) compared to untreated CNP as well as CNP treated with ALD and esterification that absorbed well over 100% of their weight in 30 seconds. These improvements confirm that both treatments are viable in the short-term on TEMPO-oxidized CNP, but further studies are needed to determine ways to

prolong the effectiveness of esterification. However, for use in full environmental conditions, these improvements are unsatisfactory and will not protect the CNP. In certain limited environments, these treatments might provide increased performance and longevity, but the in-depth manufacturing process for paper with these surface modifications would make them prohibitively expensive when compared to their performance. Other solutions are likely viable which may improve the paper further while maintaining its eco-friendly quality.

Finally, the conductive films treatment process aimed to introduce electrical conductivity to CNP by depositing conductive CNT/CNF films, for use in flexible electronics and optoelectronics applications. Two water-based conductive inks were developed, containing -COOH functionalized single-walled CNTs as well as 1-D CNF together as a sonicated suspension. Inks were created with ratios of 10:1 w/w CNT/CNF and 2:1 w/w CNT/CNF, with 5 mg/mL of CNT for both inks. Addition of CNF to the conductive inks resulted in increased transmittance but also higher sheet resistance across all samples. Transmittance values were observed to increase with a smaller CNT/CNF w/w ratio, because the CNF was observed to fill the holes in the conductive coatings. The coating of cellulose nanopaper and its derivatives showed how various surface treatments in conjunction with conductive coatings may yield optimal results ranging from 70 – 200 Ωsq^{-1} and 35 - 58% transmittance at 550 nm. CNP samples esterified with pivalic acid exhibited the lowest sheet resistance across both ink formulas. Compared to CNT films on PET with 250 – 500 Ωsq^{-1} and 88 – 91% transmittance, CNP as a substrate seems to exhibit enhanced ability to retain lower sheet resistance while PET maintains higher transmittance (Hecht et al., 2009).

Due to its porous structure, which encourages a high surface area of contact between the CNTs and paper, CNP was found to outperform plastics with CNT ink sheet resistances found to be as low as $10 \Omega\text{sq}^{-1}$ (Hu et al, 2009). These findings indicate new avenues for depositing conductive, transparent films on CNP, an insulating and fibrous material, by altering the proportion of conductive material to viscosity modifiers, with CNF being used as a novel surfactant in the conductive ink as demonstrated first by Hoeng et al. in 2016.

The findings of these research experiments can be summarized as follows:

1. The cellulose nanopaper fabrication process for pine as a starting material must be altered to successfully create CNP from jute cellulose.
2. Deposition of Al_2O_3 at 250, 500, and 1000 cycles did not have a significant impact on the cellulose nanopaper's tensile strength.
3. Cellulose nanopaper's water absorption can be reduced by 38% and 58% by esterification and ALD treatments, respectively.
4. Application of conductive ink, comprised of carbon nanotubes and cellulose nanofibers, onto the surface of the paper creates a highly conductive substrate with sheet resistance ranging from $60 \Omega\text{sq}^{-1}$ to $200 \Omega\text{sq}^{-1}$, but sacrifices transparency.

There has been a significant amount of research into CNP with the intent of fully understanding its properties and instigating an era of sustainable materials for electronics and energy devices. Conceived in 2008 by Henriksson et al., research into

this novel and green material continues today in fields even outside of electronics and energy, like patient-tailored drug delivery (Löbmann et al., 2017) and chemosensing (Pourreza, 2015). Clearly CNP holds potential beyond what has been investigated in this thesis. In order to fully realize this potential, further research and improvements, including the recommendations outlined previously, need to be made in water stability while maintaining the high strength, flexibility, transparency, and conductivity demonstrated with this research. Hopefully, the use of CNP one day becomes as ubiquitous as cellulose itself as its full potential as a material is realized.

References

- Banerjee, P.; Lee, W.-J.; Bae, K.-R.; Lee, S. B.; Rubloff, G. W., Structural, electrical, and optical properties of atomic layer deposition Al-doped ZnO films. *Journal of Applied Physics* 2010, 108 (4).
- Cao, X., Ding, B., Yu, J., & Al-Deyab, S. (2012). Cellulose nanowhiskers extracted from TEMPO-oxidized jute fibers. *Carbohydrate Polymers*, 90(2), 1075-1080. <http://dx.doi.org/10.1016/j.carbpol.2012.06.046>
- Accu Dyne Test. (2017). Critical Surface Tension and Contact Angle with Water for Various Polymers. https://www.accudynetest.com/polytable_03.html?sortby=contact_angle
- Colvin, V. L. (2003). The potential environmental impact of engineered nanomaterials. *Nature Biotechnology*, 21(10), 1166-1170.
- Das, K., Ray, D., Banerjee, C., Bandyopadhyay, N., Sahoo, S., Mohanty, A., & Misra, M. (2010). Physicomechanical and Thermal Properties of Jute-Nanofiber-Reinforced Biocopolyester Composites. *Industrial & Engineering Chemistry Research*, 49(6), 2775-2782. <http://dx.doi.org/10.1021/ie9019984>
- Elam, J. W.; George, S. M., Growth of ZnO/AL₂O₃ Alloy Films Using Atomic Layer Deposition Techniques. *Chemistry of Materials* 2003, 15, 1020-1028.
- Eldridge, J. J., Crockett, R. M., Maund, J. R., Leonard, D., Mcnaught, R. H., Li, W., ... Koester, D. (2012). Greatly Increased Toughness of Infiltrated Spider Silk. *Science*, 324, 488–492.

- Fang, Z.; Zhu, H.; Preston, C.; Han, X.; Li, Y.; Lee, S.; Chai, X.; Chen, G.; Hu, L.,
Highly transparent and writable wood all-cellulose hybrid nanostructured
paper. *Journal of Materials Chemistry C* 2013, 1 (39), 6191-6197.
- Feng, Y., Zhang, X., Shen, Y., Yoshino, K., & Feng, W. (2012). A mechanically
strong, flexible and conductive film based on bacterial cellulose/graphene
nanocomposite. *Carbohydrate Polymers*, 87(1), 644–649.
doi:10.1016/j.carbpol.2011.08.039
- Fischer, E., & Speier, A. (1924). Darstellung der ester. In *Untersuchungen aus
Verschiedenen Gebieten* (pp. 285-291). Springer Berlin Heidelberg.
- Fujisaki, Y., Koga, H., Nakajima, Y., Nakata, M., Tsuji, H., Yamamoto, T., ...
Shimidzu, N. (2014). Transparent Nanopaper-Based Flexible Organic Thin-
Film Transistor Array. *Advanced Functional Materials*, 24(12), 1657–1663.
doi:10.1002/adfm.201303024
- Groner, M. D.; Elam, J. W.; Fabreguette, F. H.; George, S. M., Electrical
characterization of thin Al₂O₃ films grown by atomic layer deposition on
silicon and various metal substrates. *Thin Solid Films* 2002, 413 (2), 186-197.
- Hajian, A., Lindström, S. B., Pettersson, T., Hamed, M. M., & Wagberg, L. (2017).
Understanding the Dispersive Action of Nanocellulose for Carbon
Nanomaterials. *Nano Letters*, 17(3), 1439-1447.
- Haggenmueller, R., Rahatekar, S. S., Fagan, J. A., Chun, J., Becker, M. L., Naik, R.
R., ... & Fox, D. F. (2008). Comparison of the quality of aqueous dispersions
of single wall carbon nanotubes using surfactants and biomolecules.
Langmuir, 24(9), 5070-5078.

- Hecht, D. S., Thomas, D., Hu, L., Ladous, C., Lam, T., Park, Y., Irvin, G., & Drzaic, P. (2009). Carbon-Nanotube Film on Plastic as Transparent Electrode for Resistive Touch Screens. *Journal of the Society for Information Display*, 17 (11), 941-946.
- Henriksson, M., Berglund, L. A., Isaksson, P., Lindstrom, T., & Nishino, T. (2008). Cellulose nanopaper structures of high toughness. *Biomacromolecules*, 9(6), 1579-1585. (10.1021/bm800038n)
- Hoeng, F., Denneulin, A., & Bras, J. (2016). Use of nanocellulose in printed electronics: a review. *Nanoscale*, 8, 13131. doi: 10.1039/c6nr03054h
- Hoeng, F., Denneulin, A., Krosnicki, G., & Bras, J. (2016). Positive impact of cellulose nanofibrils on silver nanowire coatings for transparent conductive films. *J. Mater. Chem. C*, 4(46), 10945-10954. <http://dx.doi.org/10.1039/c6tc03629e>
- Hoeng, F., Denneulin, A., Reverdy-Bruas, N., Krosnicki, G., & Bras, J. (2016). Rheology of cellulose nanofibrils/silver nanowires suspension for the production of transparent and conductive electrodes by screen printing. *Applied Surface Science*. <http://doi.org/10.1016/j.apsusc.2016.10.073>
- Hopewell, J.; Dvorak, R.; Kosior, E., *Plastics recycling: challenges and opportunities*. *Philosophical Transactions of the Royal Society, Series B, Biological Sciences* 2009, 364 (1526), 2115-2126.
- Hu, L., Hecht, D., & Grüner, G. (2010). Carbon Nanotube Thin Films: Fabrication, Properties, and Applications. *Chemical Reviews*, 110(10), 5790-5844. <http://dx.doi.org/10.1021/cr9002962>

- Hu, L., Choi, J.W., Yang, Y., Jeong, S., Mantia, F. L., Cui, L., & Cui, Y. (2009). Highly Conductive Paper for Energy-Storage Devices. *PNAS* 2009, 106 (51), 21490-21494.
- Hu, L., Kim, H., Lee, J., Peumans, P., & Cui, Y. (2010). Scalable Coating and Properties of Transparent, Flexible, Silver Nanowire Electrodes. *ACS Nano*, 4(5), 2955-2963. <http://dx.doi.org/10.1021/nn1005232>
- Hu, L., Zheng, G., Yao, J., Liu, N., Weil, B., & Eskilsson, M. et al. (2013). Transparent and conductive paper from nanocellulose fibers. *Energy Environ. Sci.*, 6(2), 513-518. <http://dx.doi.org/10.1039/c2ee23635d>
- Huang, J.; Zhu, H.; Chen, Y.; Preston, C.; Rohrbach, K.; Cumings, J.; Hu, L., Highly Transparent and Flexible Nanopaper Transistors. *ACS Nano* 2013, 7 (3), 2106-2113. doi:10.1021/nn304407r
- Hunt, R., LCA considerations of solid waste management alternatives for paper and plastics. Elsevier Science- *Resources, Conservation and Recycling*, 1995, 14, 225-231.
- Imai, M., Akiyama, K., Tanaka, T., & Sano, E. (2010). Highly strong and conductive carbon nanotube/cellulose composite paper. *Composites Science and Technology*, 70(10), 1564-1570.
- Jabbour, L., Chaussy, D., Eyraud, B., & Beneventi, D. (2012). Highly conductive graphite/carbon fiber/cellulose composite papers. *Composites Science And Technology*, 72(5), 616-623. (10.1016/j.compscitech.2012.01.006)
- Jing, M., Han, C., Li, M., & Shen, X. (2014). High performance of carbon nanotubes/silver nanowires-PET hybrid flexible transparent conductive films

- via facile pressing-transfer technique. *Nanoscale Research Letters*, 9(1), 588.
<http://dx.doi.org/10.1186/1556-276x-9-588>
- Kabir, M., Islam, M., & Wang, H. (2013). Mechanical and Thermal Properties of Jute Fibre Reinforced Composites. *Journal Of Multifunctional Composites*, 1(1).
<http://dx.doi.org/10.12783/issn.2168-4286/1.1/kabir>
- Korhonen, J. T.; Hiekkataipale, P.; Malm, J.; Karppinen, M.; Ikkala, O.; Ras, R. H. A., Inorganic Hollow Nanotube Aerogels by Atomic Layer Deposition onto Native Nanocellulose Templates. *ACS Nano* 2011, 5 (3), 1967-1974.
- Lee, Doug. "Carbon-Negative Packaging: Dell to Build PCs Reusing Plastic from Recycled Electronics." *World Industrial Reporter*. Thomas Publishing Company, 18 Aug. 2016. Web. 28 Apr. 2017.
- Lee, K.-Y.; Quero, F.; Blaker, J. J.; Hill, C. A. S.; Eichhorn, S. J.; Bismarck, A., Surface only modification of bacterial cellulose nanofibres with organic acids. *Cellulose* 2011, 18 (3), 595-605.
- Leskela, M.; Ritala, M., Atomic layer deposition (ALD): from precursors to thin film structures. *Thin Solid Films* 2002, 409 (1), 138-146.
- Löbmann, K., Wohler, J., Müllertz, A., Wågberg, L., & Svagan, A. (2017). Cellulose Nanopaper and Nanofoam for Patient-Tailored Drug Delivery. *Advanced Materials Interfaces*, 1600655. <http://dx.doi.org/10.1002/admi.201600655>
- Obeso, C. G., Sousa, M. P., Song, W., Mano, J. F., Obeso, C. G., Sousa, M. P., Song, W., ... Bhushan, B. (January 01, 2013). Modification of paper using polyhydroxybutyrate to obtain biomimetic superhydrophobic substrates. *Colloids and Surfaces A: Physicochemical and Engineering Aspects*, 416, 1,

- 51-55. Plastic Products, Inc. (2017) PET(polyethylene terephthalate) Physical Properties. <http://www.plastic-products.com/part12.htm>.
- Pourreza, N., Golmohammadi, H., Naghdi, T., & Yousefi, H. (2015). Green in-situ synthesized silver nanoparticles embedded in bacterial cellulose nanopaper as a bionanocomposite plasmonic sensor. *Biosensors And Bioelectronics*, 74, 353-359. <http://dx.doi.org/10.1016/j.bios.2015.06.041>
- Pulskamp, K., Diabaté, S., & Krug, H. F. (2007). Carbon nanotubes show no sign of acute toxicity but induce intracellular reactive oxygen species in dependence on contaminants. *Toxicology letters*, 168(1), 58-74.
- Sehaqui, H.; Zimmerman, T.; Tingaut, P., Hydrophobic cellulose nanopaper through a mild esterification procedure. *Cellulose* 2014, 21 (1), 367-382. <http://dx.doi.org/10.12783/issn.2168-4286/1.1/kabir>
- Sinha, E., & Rout, S. (2009). Influence of fibre-surface treatment on structural, thermal and mechanical properties of jute fibre and its composite. *Bulletin Of Materials Science*, 32(1), 65-76. <http://dx.doi.org/10.1007/s12034-009-0010-3>
- Stelte, W.; Sanadi, A. R., Preparation and Characterization of Cellulose Nanofibers from Two Commercial Hardwood and Softwood Pulps. *Industrial and Engineering Chemistry Research* 2009, 48 (24), 11211-11219.
- Thurber, W. Robert. Hall Effect Measurements. National Institute of Standards and Technology, Engineering Physics Division (2008).
- Wang, H.; Huang, L.; Lu, Y., Preparation and Characterization of Micro- and Nanofibrils from Jute. *Fibers and Polymers* 2009, 10 (4), 442-445

- Wang, W.-m.; Cai, Z.-s.; Yu, J.-y.; Xia, Z.-p., Changes in composition, structure, and properties of jute fibers after chemical treatments. *Fibers and Polymers* 2009, 10 (6), 776-780.
- Xu, X., Zhou, J., Jiang, L., Lubineau, G., Ng, T., & Ooi, B. et al. (2016). Highly transparent, low-haze, hybrid cellulose nanopaper as electrodes for flexible electronics. *Nanoscale*, 8(24), 12294-12306.
<http://dx.doi.org/10.1039/c6nr02245f>
- Yu, L., Jinyou Tian, Feng Li, Xiuhong Bian, Fenggang Wang, J, Cellulose nanofibrils generated from jute fibers with tunable polymorphs and crystallinity. *Journal of Materials Chemistry A* 2014, 2 (18), 6402-6411.
- Zheng, G., Cui, Y., Karabulut, E., Wågberg, L., Zhu, H., & Hu, L. (2013). Nanostructured paper for flexible energy and electronic devices. *MRS bulletin*, 38(04), 320-325.
- Zhu, H.; Fang, Z.; Preston, C.; Li, Y.; Hu, L., Transparent Paper: fabrications, properties, and device applications. *Energy & Environmental Science* 2014, 7 (1), 269-287.
- Zhu, H., Li, Y., Fang, Z., Xu, J., Cao, F., Wan, J., & Preston, C. (2014). Highly Thermally Conductive Papers with Percolative Layered Boron Nitride Nanosheets. *ACS Nano*, 8(4), 3606–3613. <http://doi.org/10.1021/nn500134m>
- Zhu, H.; Parvinian, S.; Preston, C.; Vaaland, O.; Ruan, Z.; Hu, L., Transparent nanopaper with tailored optical properties. *Nanoscale* 2013, 5 (9), 3787-3792.

Zhu, H.; Xiao, Z.; Liu, D.; Li, Y.; Weadock, N. J.; Fang, Z.; Huang, J.; Hu, L.,

Biodegradable transparent substrates for flexible organic-light-emitting

diodes. *Energy & Environmental Science* 2013, 6 (7), 2105-2111.

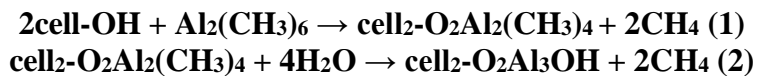
Appendices

Appendix A: Cellulose Nanopaper (CNP) Fabrication

- 1) Prepare buffer solution (Volume 4:1 of 0.1 mol/L Na_2CO_3 : 0.1 mol/L NaHCO_3)
 - a) Weigh 4.24g (0.04mol) sodium carbonate (Na_2CO_3) and 0.84g (0.01mol) sodium bicarbonate (NaHCO_3)
 - b) Use 500 ml deionized water to dilute both into 0.1 moles/L solution, stir until fully dissolved. (>5min)
- 2) Prepare oxidation solution
 - a) Using weighing paper, weigh 78.125 mg TEMPO (ultra-toxic, with mask and eye protection) and dissolve TEMPO in 25mL buffer solution.
 - b) 514.45 mg sodium bromide (NaBr) and dissolve in 50mL buffer solution.
 - c) Stirring both solution until uniform. (TEMPO takes longer than 1h.)
- 3) Weigh bleached softwood pulp.
 - a) To obtain 5g dry fiber, use following formula to determine necessary wet fiber amount: $x = 5/(100-w.p.) * 100$, x = wet pulp (g), w.p. = weight percent water (%)
- 4) Begin the reaction.
 - a) Mix the wet fiber pulp with NaBr and TEMPO solution from step 2
 - b) Add 115g buffer solution and stir at the speed of 700rpm using IKA Ultra Turrax mixer for 10min
 - c) Weigh 35mL (1mL = 1g) sodium hypochlorite (NaClO). Then, add NaClO solution dropwise into pulp suspension and begin to record the reaction time
 - d) During the reaction, pH is controlled at 10.5 with 3 moles/L sodium hydroxide (NaOH , highly basic) solution. The pH is monitored at intervals of 15 min, and add 15 drops NaOH into the solution. The reaction will last for at least 2 hours
 - e) Remain stirring the solution for additional 12 hours
- 5) Wash the reactant
 - a) While the reaction finishes, transfer the fibers dispersion into Büchner filtration to remove the reactive agents and water.
 - b) After filtration, transfer the residual gel-like fibers to beaker with 1L volume of distill water and stir for 5 min at speed of 500 rpm/min to re-dissolve the fibers.
 - c) Repeat the step a-b washing for a total of 3 times.
- 6) Microfluidize solution
- 7) Perform casting
 - a) Place smooth tray (8.5in x 11in) in casting chamber
 - b) Pour filtered solution containing 5g of dry fiber into casting tray
 - i) If tray is not 8.5 x 11 in, calculate adjusted amount of fibers required
 - c) Adjust conditions in chamber as needed. Remove tray when completely dry

Appendix B: Atomic Layer Deposition (ALD) Process Specifications

Using a BenEq TFS 500 ALD machine, the reaction equations and process specifications for Al₂O₃ deposition are as follows:



The growth per cycle (GPC) is 0.09-0.11 nm on silicon. The reaction sequence above is followed by a distilled water pulse cycle and nitrogen gas purge cycle at a 1:2 pulse to purge ratio.

Appendix C: Carbon Nanotube (CNT) Ink Formula and Preparation

- 1) Prepare CNF dispersion by normal TEMPO oxidation procedure
- 2) Prepare conductive ink
 - a) Functionalized CNT w/ CNFs as surfactant [Ink 1]
 - i) Add –COOH functionalized CNTs (P3, Carbon Solutions) to CNF solution with a concentration of 5 mg CNT/mL
 - ii) Add CNF dispersion (surfactant) to achieve 50 mg CNTs, 25 mg CNFs (2:1 w/w CNT/CNF)
 - iii) Bath sonicate for 10-15 minutes
 - iv) Probe sonicate for 5 minutes (500 W, 20 kHz probe)
 - (1) 1s on, 5s off duration for 5 minutes, 30% amplitude
 - b) Functionalized CNT w/ CNFs as surfactant [Ink 2]
 - i) Add –COOH functionalized CNTs (P3, Carbon Solutions) to CNF solution with a concentration of 5 mg CNT/mL
 - ii) Add CNF dispersion (surfactant) to achieve 50 mg CNTs, 5 mg CNFs (10:1 w/w CNT/CNF)
 - iii) Bath sonicate for 10-15 minutes
 - iv) Probe sonicate for 5 minutes (500 W, 20 kHz probe)
 - (1) 1s on, 5s off duration for 5 minutes, 30% amplitude
- 3) Mechanically press CNP substrate for 24 hours before rolling for flat, even surface
- 4) Deposit a single conductive coating with 100 microliters of ink for a ~4 cm² sample by dragging with #12 Meyer rod
- 5) Mechanically press coated CNP samples for 24 hours

Glossary

Aerogels: porous, solid materials with characteristically low densities

Anhydride: the compound obtained by removing the elements of water from a compound

Agglomeration: grouping or clumping of particles when suspended in mixture or solution

Aspect ratio: ratio of the length or depth of a hole (in which a wire is inserted to connect to a circuit) to its pre-plated diameter

Atomic force microscopy (AFM): a very-high-resolution type of scanning probe microscopy (SPM), with demonstrated resolution on the order of fractions of a nanometer

ATR-IR: Attenuated total reflection (ATR) is a sampling technique used in conjunction with infrared (IR) spectroscopy, which enables samples to be examined directly in the solid or liquid state

Bending radius: the minimum radius one can bend a pipe, tube, sheet, cable or hose without kinking it, damaging it, or shortening its life

Biocopolyester: a biological composite material consisting of agricultural products in a polymer (polyester) matrix

Buchner funnel: a cylindrical, porcelain funnel for filtering processes that has a perforated plate on which the flat filter paper is placed

Cellulose: a naturally occurring polysaccharide consisting of chains of glucose monomers; the main constituent of plant cell walls and of vegetable fibers

Cellulose nanofibers (CNF): cellulose that has undergone mechanical and chemical processes to decrease the fiber size to the nanoscale (10^9)

Conformal deposition method: a technique such as chemical vapor deposition or atomic layer deposition that results in a morphologically uneven interface with a substrate, also with a uniform thickness across the entire interface

Degree of polymerization: the average number of monomeric units in a polymer chain; describes the typical length of a polymer with respect to its constituent **monomers**

Fourier transform infrared spectroscopy (FTIR): a technique that is used to obtain an infrared spectrum of absorption or emission of a solid, liquid or gas, particularly in organic chemistry

Functionality: specifically, electrical functionality, the ability for the prepared material to serve as a circuit element

Hall effect: The production of a voltage difference across an electrically conductive material in the direction opposite to (1) a propagating electric current in the conductor and (2) a magnetic field; the **Hall coefficient** is the ratio of the induced electric field to the product of the current density and the applied magnetic field, and is an intrinsic material property

Hemicelluloses: members of a class of substances found in cell walls of plants; polysaccharides with a simpler structure than cellulose

Hierarchical structure: in paper, the nested arrangement of fibers that can be reduced to increasingly smaller units (e.g. a micro fiber is composed of many nanofibers)

Hot pressing: a high-pressure, low-strain-rate process at an elevated temperature that produces a smooth surface on paper

Hydrogen bonding: dipole-dipole secondary bonding between two molecules resulting from electrostatic attraction between a proton in one molecule and an electronegative atom in another

Hydrophilic: tending to mix with, dissolve in, or be wetted by water

Hydrophobicity: tending to repel or fail to mix with water (opposite of hydrophilicity)

Inhomogeneity: the quality of being not uniform in character or content

Life cycle assessment: a tool used to assess the environmental impacts of a product, process or activity throughout its life cycle: from the extraction of raw materials through to processing, transport, use and disposal.

Lignin: a complex organic polymer deposited in the cell walls of many plants, making them rigid and woody.

Low-dimensional [material]: systems in which electronic state **wave function** is confined, at least in one of the three dimensions, on a range of 1 nm to 100 nm.

Mechanical film adhesion: the ability of an applied film (e.g. CNT ink) to remain on the substrate in the presence of an upward “peeling” force

Meyer rod: a metal rod that has fine wire around the central axis so that liquids can be drawn down evenly at a given thickness across a substrate

Microfiber Angle: the angle that the microfiber makes with the length of the macro-sized fiber

Monomer: a fundamental molecule that can be bonded to other identical molecules to form a polymer

Optical haze: a percentage used to quantify the amount of forward scattered light in a transparent material; has significance in solar cell applications where cellulose nanopaper is the substrate

Oxidation: a chemical reaction in which a material gives up electrons, typically gaining an oxygen atom

Packing density: degree of compactness in sub-components

Photovoltaic: describing any device that produces an electric current and the junction of two materials exposed to light.

Polar: having distinct partial charge

Porosity: the measure of the void or empty spaces in a material, expressed as a fraction of the volume

Precursor: one of several chemicals that react with the substrate to build up layers of the deposited material

Pressurization: to confine the contents of a vessel under a pressure greater than that of the outside (atmospheric) pressure

Roll-to-roll printing: in the field of electronic devices, the process of continuously creating electronic devices on a roll of flexible plastic, metal foil or another substrate

Scanning electron microscopy (SEM): a device in which the specimen is examined point by point directly in a moving electron beam; electrons reflected by the specimen are used to form a magnified, three-dimensional image

Scattering: the process in which electromagnetic radiation, particles, or other atomic entities are deflected or diffused from a straight trajectory

Secondary electron: electrons generated from the material by outside radiation as a product of ionization

Semiconductor: a material with electrical conductivity between that of a conductor such as copper and that of an insulator such as glass

Sheet resistance: measure of electrical conductivity for thin coatings of material; measured in ohm/square of material

Single-walled carbon nanotubes (CNT): long, thin tube-shaped molecules of pure carbon that are about 1-3 nm in diameter and hundreds to thousands of nanometers long; specifically, the wall of the tube is composed of a single layer of 2D carbon

Sonication: the process of applying sound energy to a sample to agitate particles in the sample

Spectrophotometer: instrument used to measure light transmittance

Strain-to-failure ratio: the measure of how long the specimen can elongate before failure

Strain neutral: the neutral axis in the cross section of a beam (a member resisting bending) or shaft along which there are no longitudinal stresses or strains

Substrate: a substance or layer on which some process occurs, i.e. growth or deposition

Surface free energy: the excess energy at the surface of a material compared to the bulk, also known as the work which must be expended to increase the size of the surface

Surfactant: a substance that reduces the surface tension of a liquid into which it is dissolved

TEMPO-oxidation: a cellulose fiber processing method involving the use of (2,2,6,6 - Tetramethylpiperidin-1-yl)oxidanyl, also known as TEMPO, to break hydrogen bonds holding cellulose fibers together, resulting in a smaller fiber size

Tensile strength: the resistance of a material to breaking under tension

Topology: the way in which constituent units are interrelated or arranged

Transmittance: percent of light that can pass through a material

UV-Vis spectroscopy: absorption spectroscopy in the ultraviolet-visible spectral region

Van der Pauw technique: a technique used to measure the resistivity and **Hall coefficient** of a two-dimensional sample by calculating average resistivity between four probes placed at the perimeter of the sample

Viscosity modifier: polymer additives that contract and relax in solution to alter the viscosity of a fluid solvent

Wave function: a mathematical function that describes the quantum state of the system.

Wettability: the tendency of a fluid to spread on or adhere to a solid surface; the interaction between fluid and solid phases

Young's modulus: a measure of elasticity, equal to the ratio of the stress acting on a substance to the strain produced